Integrated Torque Vectoring and Path Following using Non-linear Model Predictive Control

Klait Bani

Delft University of Technology

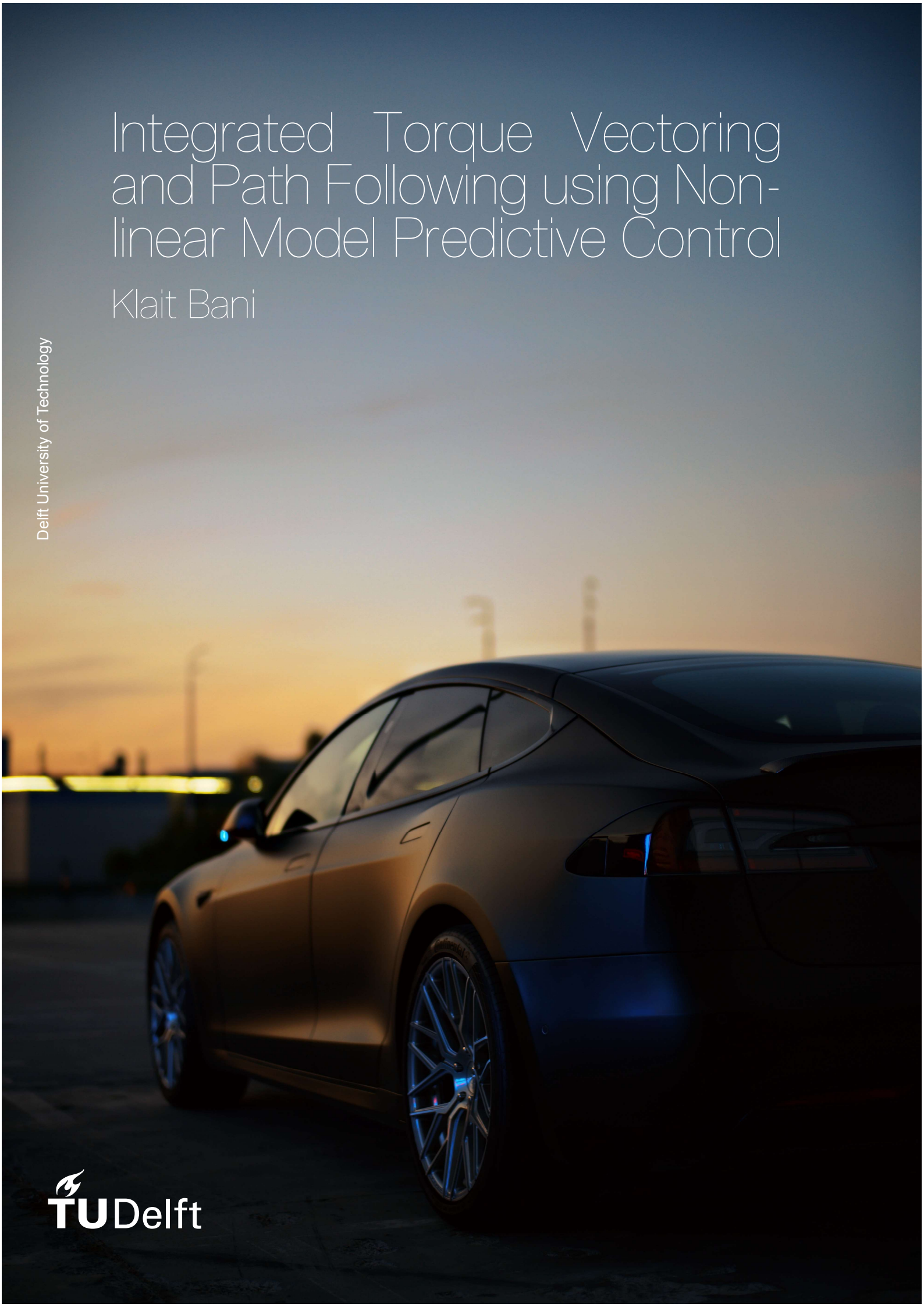

TU Delft

Integrated Torque Vectoring and Path Following using Nonlinear Model Predictive Control

by

Klait Bani

To obtain the degree of Master of Science in Mechanical Engineering
at the Delft University of Technology,
To be defended publicly on Tuesday October 31, 2023 at 14:00 PM.

Student number: 4468716

Thesis committee:	Prof. dr. ir. G. Papaioannou,	TU Delft, CoR-IV
	Dr. ir. B. Shyrokau,	TU Delft, Supervisor, Assistant Professor, CoR-IV
	Mr. A. Bertipaglia,	TU Delft, PhD Student, CoR-IV

TU Delft Delft University of Technology

Cognitive Robotics

Abstract

This thesis introduces a novel model predictive controller (MPC) that integrates both torque vectoring and path following into one controller. Due to a need to improve vehicle safety, systems are being developed in order to improve vehicle handling. One system that is able to improve the vehicle handling is torque vectoring (TV). With torque vectoring, the magnitude and the direction of torque can be controlled by either applying the motor or brake torques. Additionally, in order to eliminate human error as a cause of accident, automated drive (AD) vehicles are being developed. A key task for AD vehicles is to perform path following (PF), where the vehicle follows a predetermined reference path generated by path planning.

Beforehand, these tasks were performed by separate controllers, where one controller performed path following and the other controller focused on torque vectoring. The disadvantage of this method is that it leads to sub-optimal results as both controllers have opposing objectives. The TV controller is able to decrease the steering angle in order to improve the vehicle handling, whereas the PF controller could require a higher steering angle in order to follow the path. By integrating both tasks, the novel controller is able to optimise the control output such that both objectives are achieved.

The use of model predictive control strategies with TV have been studied and its ability to deal with hard constraints, while decreasing the state errors and control input, makes it a suitable choice to use it for TV. When the MPC strategy is compared to more common control strategies it is clear that the MPC TV algorithm provides better results in terms of responsiveness, lateral acceleration and vehicle handling. Furthermore, due to its ability to integrate multiple applications and its ability to handle a greater level of complexity, a nonlinear model predictive control (NMPC) formulation will be used to perform both torque vectoring and path following.

In order to test the new MPC controller, benchmark controllers have been created for comparison. The benchmark controllers are two controllers that are able to perform torque vectoring by generating a corrective yaw moment to follow the yaw rate reference. The torques are then allocated based on the size and direction of the corrective yaw moment. Then, the NMPC controller that performs path following by using both the steering angle and torques as an input will be compared to a controller that is able to perform path following by using the steering angle as an input.

The controllers are compared by using the sine with dwell test and the double lane change manoeuvre. These manoeuvres are used to test the lateral performance, vehicle handling, responsiveness and tracking performance of the vehicles. Key performance indicators (KPI) are used in order to evaluate the results regarding tracking performance and the vehicle handling.

The results show that the NMPC controller has an increase in performance regarding both path following and vehicle handling. When compared to the benchmark torque vectoring controller, the vehicle handling is increased by 5% and the lateral performance is increased by 6 %. Additionally, compared to the path following controller, by adding torque vectoring, the NMPC controller has improved the path following by 4 %, the vehicle handling has been improved by 5 % and the responsiveness has been improved by 11 %.

Contents

List of Symbols

$G_{yaw,\delta}^{ss}$ Steady-state yaw rate gain from steering angle [-]

$G_{yaw,Mz}^{ss}$ Steady-state yaw rate gain from yaw moment generated by TV [-]

α Tyre slip angle [deg]

β Sideslip angle [rad]

ΔF_z^x Longitudinal load transfer [N]

ΔF_z^y Lateral load transfer [N]

ΔT_f Front-to-total torque distribution factor [-]

δ Steering angle [rad]

$\dot{\delta}$ Steering rate [rad/s]

$\dot{\psi}$ Yaw rate [rad/s]

$\dot{\psi}_{ref}$ Yaw rate reference [rad/s]

μ Tyre-road friction coefficient [-]

ω angular wheel velocity [rad/s]

$\omega_{n,0}$ Yaw time delay [s]

ω_n Natural yaw frequency [s^{-1}]

σ Longitudinal slip ratio [-]

Θ Parameter vector

ζ Yaw damping ratio [-]

a_x Longitudinal acceleration [m/s^2]

a_y Lateral acceleration [m/s^2]

$C_{\alpha,r}$ Rear cornering stiffness [N/rad]

dM_z Additional yaw moment [Nm]

$e_{\dot{\psi}}$ yaw rate error [rad/s]

e_{Tr} Rear-to-total torque distribution [-]

e_x Longitudinal error [m]

e_y Lateral error [m]

F_x Longitudinal force [N]

F_y Lateral force [N]

h_{CG} Centre of gravity height [m]

h_{roll} Roll centre height [m]

$IA_{\delta_{SW}}$ Normalised integral of the absolute value of the steering angle [deg]

$IA_{M_{z,ref}}$ Normalised integral of the absolute value of the reference direct yaw moment [Nm]

J Cost function

K_{us} Understeer gradient [deg/g]

L Feedback matrix of the LQR state controller

l_f Distance between the front axle and the horizontal CoG position of the vehicle [m]

l_r Distance between the rear axle and the horizontal CoG position of the vehicle [m]

L_w Wheelbase [m]

m Vehicle mass [kg]

M_z Yaw moment [Nm]

$M_{z,R}$ Targeted yaw moment value [Nm]

$M_{z,TV}$ Yaw moment generated by torque vectoring [Nm]

N_c Control horizon

N_p Prediction horizon

P Solution of discrete algebraic Ricatti equation

p_a Acceleration input from driver [%]

p_b Braking input from driver [%]

P_{Loss} Power loss [kW]

Q Cost function state feedback matrix

R Wheel radius [m]

r_u Ratio of weighting coefficient [-]

r_{ref} Yaw rate reference [rad/s]

s_x Longitudinal slip [-]

s_y Lateral slip [deg]

SR Steering ratio [-]

T Wheel torque [Nm]

T_p Prediction time [s]

T_s Sampling time [s]

t_w Track width [m]

T_w^{tot} Total wheel torque [Nm]

u Input vector

$u(k)$ MPC inputs

U_{sc} Scaling factor coefficent [-]

V Total vehicle velocity [m/s]

V_x	Longitudinal vehicle velocity [m/s]
V_y	Lateral vehicle velocity [m/s]
$v_{x,slip}$	Longitudinal slip velocity [m/s]
$v_{y,slip}$	Lateral slip velocity [m/s]
W_u	MPC cost function weight
X	State vector
$x(k)$	MPC states

Abbreviations

2WD 2-Wheel Drive.

AD Automated Drive.

ADAS Advanced-Driver-Assistance-Systems.

AWD All-Wheel Drive.

CoG Centre of Gravity.

DLC Double Lane Change.

ESC Electronic Stability Control.

FWD Front-Wheel Drive.

IWM In-Wheel Motor.

KPI Key Performance Indicator.

LQR Linear Quadratic Regulator.

LTV Linear-Time Varying.

MPC Model Predictive Control.

NMPC Nonlinear Model Predictive Control.

OCP Optimal Control Problem.

PF Path Following.

PID Proportional-Integral-Derivative.

QP Quadratic Programming.

RMS Root Mean Square.

RWD Rear-Wheel Drive.

SwD Sine with Dwell.

TV Torque Vectoring.

List of Figures

1 Introduction

Over the past decade vehicle safety has been improved. Between 2009 and 2014, the amount of vehicle deaths has been decreased by 11% [1]. One large contributor of this is the advanced driver-assistance systems (ADAS). These systems help the driver perform difficult manoeuvres and keep the vehicle stable during unsafe conditions. One of these systems is called torque vectoring, which increases the lateral capability of the vehicle by adding a yaw moment, making the vehicle safer at the limit of handling. In order to enhance vehicle safety even further, there has been the introduction of automated drive vehicles. One of the tasks of the AD vehicles is to perform path following safely. This chapter will introduce toque vectoring and path following for AD vehicles, which is then followed by the objective of the thesis and an outline of the structure.

1.1. Torque Vectoring Control systems

There are systems that focus on improving the lateral handling of the vehicle. An important factor for the lateral dynamics of the vehicle is the yaw response. In order to control the yaw response several yaw moment control strategies have been developed to improve vehicle stability during lateral manoeuvres. These control strategies are mostly either brake or traction torque-based. Brake-based strategies, like the electronic stability control (ESC), apply unequally distributed brake forces to stabilise the car during extreme manoeuvres. Traction-torque-based systems, such as TV, distribute torque between the left and right wheels for a two-wheel driven vehicle (2WD), such as a front-wheel drive (FWD) or rear wheel drive (RWD) and distribute torque between the front and rear wheels for an all-wheel drive (AWD). Without per-wheel motors, this is done using a limited-slip differential. Nowadays, with the introduction of electric powertrains and in-wheel motors (IWM), systems have been developed to supply torque independently to each wheel. The ability to supply torques to each wheel individually allows for a high level of controllability, as the size and magnitude for each wheel is now controlled. This can be seen in figure 1.1, where the direction and magnitude of the torques are depicted by the arrows on the wheels. Another advantage of TV systems is the ability to stabilise the vehicle in both normal driving conditions, as well as extreme driving conditions.

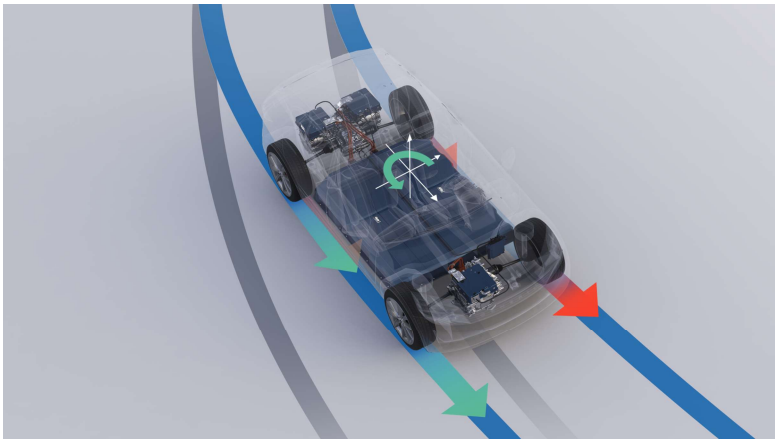

Figure 1.1: AWD torque vectoring based on yaw moment [2]

1.2. Path Following

One of the most important things an AD vehicle has to do is be able to perform path following safely. The premise of this is that the vehicle is given a reference path which it needs to follow. The aim for the vehicle is to follow the reference path as accurately as it can. This is essential as the vehicle needs to follow the path while dealing with avoiding obstacles and adapting to changing environments. Inputs that are commonly used in order to follow the path are the steering wheel for lateral PF and the throttle and brake in order to control the longitudinal velocity. In the real world a reference path is not always given, which is why a path planner is needed to generate the path and sensors are required to detect obstacles. However, as this thesis is not focused in path planning but rather in path following, the reference path will be predetermined.

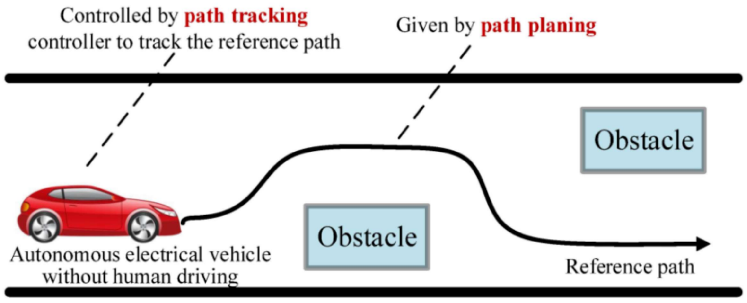

Figure 1.2: Path following example [3]

1.3. Objective and motivation

Intensive research has been done on torque vectoring, where different scenarios and control strategies have been explored. The same is applicable for path following. Nevertheless, there has been limited research in integrating torque vectoring and path following into one controller. As the computational power has increased over time, the use of nonlinear model predictive control (NMPC) has been enabled. NMPC has been researched for torque vectoring and path following alone, but no NMPC controller has been developed using both of these applications.

In order to achieve safe driving in dangerous situations, there are two important objectives for the vehicle, path following and yaw stability. As a TV controller is able to stabilise the vehicle is normal conditions and a PF controller is able to follow a path, the next step is to combine both torque vectoring and path following to perform those tasks. In most of the research, the TV controller is used as an independent controller, which receives the steering angle from the PF controller and then generates a reference yaw rate which the TV controller needs to track. While this ensures the path will still be

tracked, it can lead to a sub-optimal use of torque vectoring, which can lead to decreased agility of the vehicle. One solution is combine both controllers into one integrated controller, where the steering angle and torques are given as inputs, then both the reference path and yaw rate reference need to be tracked. The benefit of this is that with the help of weight tuning, the designer can then prioritise whether the focus should be on path following or torque vectoring. Another benefit is that the yaw rate can now be directly controlled and constrained, which can prevent a possible yaw rate tracking overshoot.

This can be done by using NMPC, which is why the focus of this thesis is to design a NMPC controller that implements both path following and torque vectoring functionality. In order to compare the NMPC controller to state of the art controllers, two benchmark controllers have been created. The benchmark controllers consist of a PD controller and a LQR controller, which is similar to what can be found in the literature.

1.3.1. Goals of the thesis

The main goal of this thesis listed below is:

Design and evaluate nonlinear model predictive controller that implements both torque vectoring and path following functionality for an AD vehicle to be able to perform in different scenarios

In order to accomplish this aim, the following sub goals were formulated:

- Design a NMPC controller that is able to perform a manoeuvre using TV.
- Create and tune 2 benchmark controllers for TV.
- Compare the NMPC controller against the benchmark controllers in terms of TV capability.
- Design the test scenarios and select the target key performance indicators to compare the controllers.
- Design a reference yaw rate based on the steering angle and the yaw moment generated by TV that the vehicle should follow.
- Develop the proposed controller that implements both torque vectoring and path following.
- Perform the simulations in Simulink/ IPG CarMaker for the different controllers and analyse the results.

1.3.2. Thesis contribution

The contribution of this thesis is a novel controller which implements both torque vectoring and path following functionality using nonlinear model predictive control. The controller is able to focus on improving the vehicle handling whilst being able to follow a reference path.

Additionally, there is also a yaw moment that has been added by torque vectoring. As this has an effect on the vehicle dynamics, the contribution of the additional yaw moment denoted by $M_{z,TV}$ has also been implemented in the steady-state yaw rate reference. This is another novel thesis contribution.

Furthermore, the bicycle model is used to determine the steady-state yaw rate reference for simplification. The steady-state yaw rate is constrained and then adjusted by the nonlinear response, which incorporates dynamics.

1.4. Outline

The thesis is structured in 8 chapters as follows:

- In chapter 2 the findings of the literature report are introduced. Here, the principles of torque vectoring and model predictive control will be introduced. Then, the report investigates the different ways how torque vectoring and model predictive control are combined in the literature and as follows the report looks into the way path following is used in the literature.
- In chapter 3 the controller design for the NMPC TV controller is shown. The vehicle, tyre and internal model is introduced, as well as the control structure, optimal control problem (OCP) formulation and the implementation.
- In chapter 4 the controller design for the NMPC with PF TV controller is shown. The structure of this chapter is similar to that of chapter 3.
- In chapter 5 the benchmark controllers are introduced with its layout and constraints.
- In chapter 6 the scenarios and KPIs that will be evaluated are introduced.
- In chapter 7 the results of the simulations of all controllers and different manoeuvres and conditions will be shown and discussed.
- In chapter 8 the conclusions and recommendations for subsequent work will be given.

2

Findings from literature

2.1. Torque Vectoring

One way of enhancing the vehicle stability is to control the yaw moment. A control system checks if the yaw rate of the vehicle matches the desired yaw rate that is based on the steering angle. If there is a large difference due to understeer or oversteer, a stabilising yaw moment is generated to make the vehicle neutral steered. This is where torque vectoring is applied. With TV, a driveline device is capable of controlling the magnitude and direction of torque to influence traction and vehicle dynamics. This can be described as a variable torque bias coupling [4]. A TV controller is able to distribute the torque independently to each wheel depending on the configuration of the vehicle, whereas a differential is limited in the torque distribution. Furthermore, with the introduction of electric powertrains, it is possible to design per-wheel motors, which enables the controller to supply the power to each wheel directly. Traditional powertrains on the other hand require sophisticated limited-slip differentials to distribute the torque. Another benefit is that per-wheel motors allow for simple power distribution for front to rear and left to right, which is not possible with front and rear differentials. Additionally, due to TV stabilising the vehicle in high grip conditions, TV results in an increase of lateral performance, responsiveness and stability as is explained in [5].

An advantage of TV is demonstrated when compared to a vehicle without TV [5]. The vehicle turns in a left-hand corner. Without TV, the vehicle becomes understeered as the front wheels have reached their friction limit. As a result, the inside wheels cannot generate enough lateral force. When TV is applied, the system distributes more torque to the right rear tyre of the vehicle and reduces the torque on the front wheels, which reduces the understeer. As the understeer is now decreased, the vehicle responsiveness increases, as well as the maximum lateral acceleration, which can be seen in figure 2.1. The maximum lateral acceleration has increased from $0.7g$ to $1g$. This has improved the vehicle performance at the friction limit for steady-state cornering.

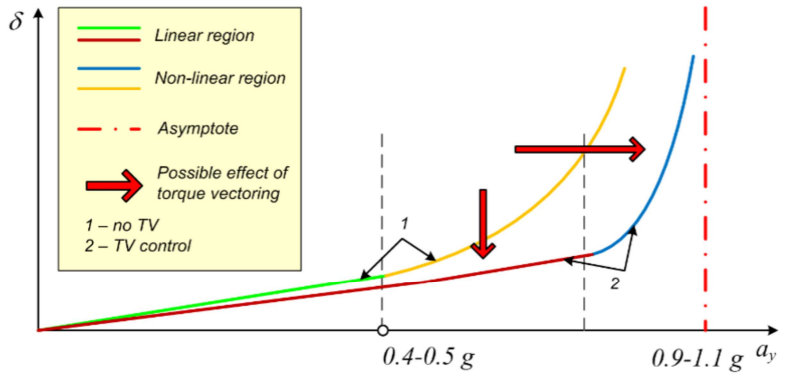

Figure 2.1: Torque Vectoring influence on understeer gradient of the vehicle

Apart from the impact TV has on the handling at the friction limit of the vehicle, it also has an impact on other driving dynamics. At the step steering manoeuvre seen in figure 2.2, it can be seen that the peak response time is reduced by approximately 30 %, due to the fast actuator speed, which confirms the increase in responsiveness. The enhancement of the steering response can be seen by the increase of yaw rate gain, which leads to the vehicle becoming more agile. The TV controlled vehicle also has a reduction in overshoot, which leads to a reduction of undesired yaw rate response and a reduction of body motion [6].

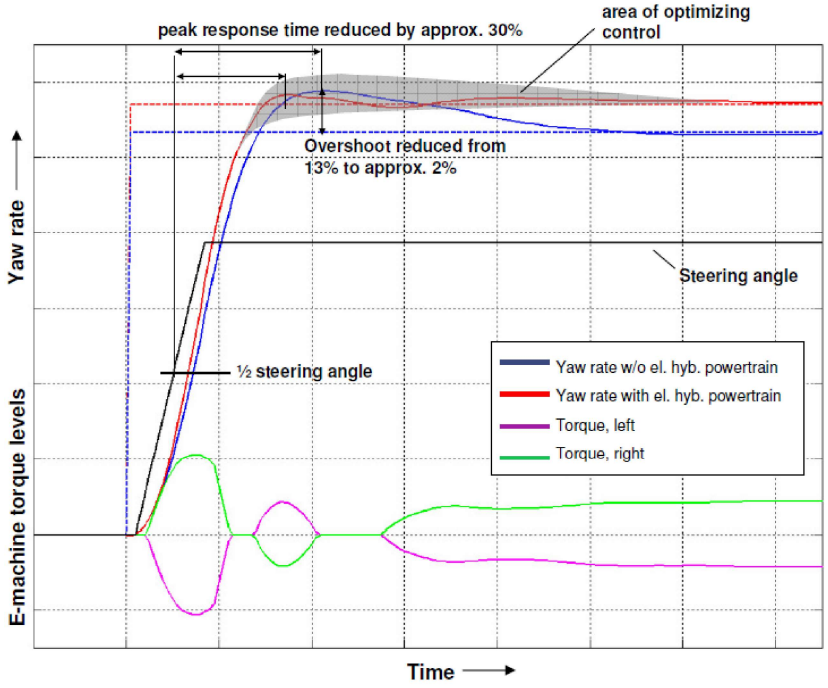

Figure 2.2: Step response comparison between a vehicle with TV control (red) and a vehicle without TV control (blue) [6]

2.2. Path Following

Most of the path following studies focus on using steering actuation as an input, as can be seen in the survey in [7]. Some of the path tracking methods are geometry based, whereas other methods are based on conventional feedback controllers like PID or LQR and simpfied vehicle dynamics models. The geometry based path tracking methods are suitable for slow driving, smooth highway driving or parking manoeuvres, whereas the feedback based controllers are suitable for urban driving at speed and highway driving. MPC is commonly utilised to perform path following because of its ability to handle future trajectories and system constraints. In [8], a NMPC and a linear time-varying MPC (LTV-MPC) controller are proposed, which controls the front steering angle. The NMPC uses the yaw angle and lateral position as system outputs. The LTV-MPC also uses the yaw rate as a system output and the steering angle as an input.

Furthermore, research has been made into combining both torque vectoring and path following. In one of the papers [9] , the performance of different path tracking controllers with integrated or separate torque vectoring functionality during obstacle avoidance tests are compared. Here it is shown that active torque vectoring control, with either integrated or separate multi-layer implementations, improved the vehicle performance, by increasing the maximum entry speed while keeping the vehicle stable, compared to path tracking control that is only based on steering system actuation. Additionally, the use of smooth reference path, similar to the path followed by the preview controllers, increases the maximum entry speed achievable with the controllers without preview, at the expense of increased oscillations after the vehicle returns to the original lane. When comparing the controllers with the separate TV with the controllers with integrated TV, the integrated steering and yaw moment controllers achieved higher entry speeds, which enhanced the vehicle agility.

Next, the performance of different types of path tracking model predictive controllers is compared in [10]. Here, there are 2 one-level controllers that solve the optimal control problem using MPC. One of these controllers applies TV, whereas the other controller allocates the torques equally among all wheels. Then, there are also 2 two-level controllers, where the upper level consists of a MPC controller that determines the forces and the yaw moment and a low-level torque allocator, which reduces the complexity of the optimisation problem, thus decreasing the computational cost. The difference between the 2 controllers is that one uses an optimisation-based algorithm to allocate the torques and the other uses a rule-based torque allocation strategy. When all of these controllers where compared, the one-level TV controller produced the highest passing velocity in all road conditions, but had degrading yaw rate tracking when the road friction varied. Whereas the two-level controllers performed more consistently when the road condition changed. Between the two-level controllers, the tracking accuracy and the passing velocity was similar even though the rule-based algorithm was easier to implement. However, the optimisation-based controller had more degrees of freedom in designing the cost function and tuning the weighting matrices.

2.3. Model Predictive Control

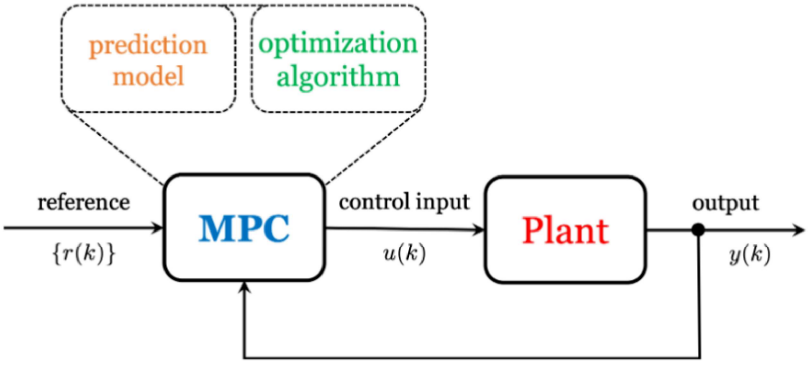

Figure 2.3: General MPC structure

Model predictive control is an advanced control method that exploits a plant model (figure 2.3) to predict its likely future output and to compute the best control input in current time. For this process, the MPC controller tries to minimise the difference between the reference output and the predicted output by means of optimisation. The optimisation is achieved within a finite-time window based on the states at the beginning of the time window. The number of time steps that the controller must evaluate by prediction is called the prediction horizon (N_P). The prediction time (T_P) is then determined by the sampling time (T_S) and the prediction horizon in (2.1).

$$T_P = N_P * T_S \tag{2.1}$$

Whereas the control horizon (N_C) is the number of time steps where the optimal control input is calculated of which its value lies between 1 and N_P ($N_C \leq N_P$). An increase of control and/or prediction horizon makes the MPC problem more complex, which leads to an increase of computational time. Figure 2.4 shows the MPC process described above as well as the prediction horizon. The length control input (denoted by Predicted Control Input) in the figure shows the control horizon, which in the figure is the same size as the prediction horizon.

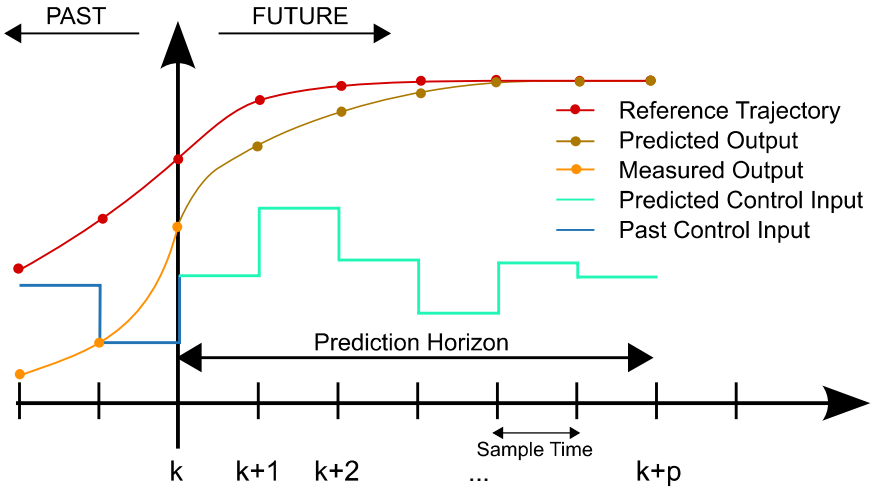

Figure 2.4: Representation of the MPC scheme [11]

In order to optimise the control input, a cost function is created. The standard cost function in (2.2) for MPC tries to minimise both the tracking error and the control input along the horizon, while staying within the state (denoted by *x*) and input (denoted by *u*) constraints.

$$V_N(x_0, u) = \sum_{k=0}^{N-1} \{\ell(x(k), u(k)\} + V_f(x(N)) \tag{2.2}$$

s.t.

$$x \in \mathbb{X}$$
$$u \in \mathbb{U}$$

The cost function consists of a stage cost given in (2.3), denoted by $\ell(x(k), u(k))$, which is a quadratic function that minimises the error between the reference output and the predicted output and to use the control input at all time steps, and a terminal cost given in (2.4), denoted by $V_f(x(N)))$, which is a penalty of the state and control input at the final time step. The terminal cost function is implemented to ensure the system is stable.

$$\ell(x(k), u(k)) = (x(k) - x_{ref})^T Q(x(k) - x_{ref}) + (u(k) - u_{ref})^T R(u(k) - u_{ref}) \tag{2.3}$$

$$V_f(x(N)) = (x(N) - x_{ref})^T P(x(N) - x_{ref}) \tag{2.4}$$

2.4. MPC Torque Vectoring Control

2.4.1. MPC linearisation

Commonly the way that MPC TV is implemented is by using simplified linearised or nonlinear prediction models. An example of linearising a nonlinear continuous-time system, taken from [12] will be shown. A nonlinear continuous-time system with state vector *x*, input vector *u* and output vector *y* is given where:

$$\dot{x} = f(x, u), \quad y = g(x, u) \tag{2.5}$$

are linearised around the equilibrium point (x^{ss}, u^{ss}, y^{ss}), which gives:

$$\dot{\tilde{x}} = A_c\tilde{x} + B_c\tilde{u}, \quad \tilde{y} = C_c\tilde{x} + D_c\tilde{u} \tag{2.6}$$

where the state, input and output errors from the equilibrium points are given by $\tilde{x} = x - x^{ss}, \tilde{u} = u - u^{ss}$ and $\tilde{y} = y - y^{ss}$. In addition, there is the associated cost function state matrix (Q_c), input weighting matrix (L_c) and the cross-weighting matrix (M_c). Discretising this system using an exact discritisation and sampling time T_s gives:

$$\tilde{x}_{k+1} = A_d\tilde{x}_k + B_d\tilde{u}_k, \quad \tilde{y}_k = C_d\tilde{x}_k + D_d\tilde{u}_k \tag{2.7}$$

A_d, B_d, C_d and D_d are the discretised equivalents of the Jacobian matrices obtained from the linearisation.

Assuming then that there is no feed through term ($D_d = 0$) and full state feedback ($C_d = I^n$), the MPC regulation problem with horizon $N = N_p = N_u$ is given by:

$$min \quad \tilde{x}_N^T P\tilde{x}_N + \sum_{k=0}^{N-1} (\tilde{x}_k^T Q\tilde{x}_k + \tilde{u}_k^T L\tilde{u}_k + 2\tilde{x}_k^T M\tilde{u}_k) \tag{2.8}$$

with the following constraints:

$$\begin{aligned} x_0 &= x_{in} \\ \tilde{x}_{k+1} &= A_d\tilde{x}_k + B_d\tilde{u}_k \\ x_k &\leq x_k \leq \bar{x}_k \\ x_k &\leq x_N \leq \bar{x}_k \\ u_k &\leq u_k \leq \bar{u}_k \end{aligned} \tag{2.9}$$

The terminal cost $\tilde{x}_N^T P \tilde{x}_N$ ensures closed loop stability [13], where matrix P is the solution of the discrete algebraic Ricatti equation:

$$P = A_c^T P A_c + Q(B_c^T P A_c + M^T)^T (L + B_c^T P B_c)^{-1}(B_c^T P A_c + M^T) \tag{2.10}$$

2.4.2. Linear MPC control

MPC is suitable to use for torque vectoring as it is able to take the torque and torque rate limit into account, while using current state measurements, state predictions and satisfying constraints on states and control inputs.

Two MPC controllers are linearised around a nonlinear system in [12]. The first controller is the *MPCt*, that uses a linearised version of full vehicle model with the vehicle velocity, sideslip angle, yaw rate and rear wheel velocities as states and the rear wheel torques as input. The cross-weighting matrix M_c is set to 0 and the weighting matrices Q_c and L_c are normalised with the respect to the state and input vectors, where the only tuning parameter is q_v. The state constraints are imposed for the yaw rate, to avoid large yaw rate values and the side slip angle as function of the velocity. There is also a longitudinal slip constraint for stability reasons, which is rewritten as a function of all states. Then, there is an input constraint for the maximum torque achievable on the two rear wheels for the vehicle, which is a nonlinear function of the corresponding wheel speed.

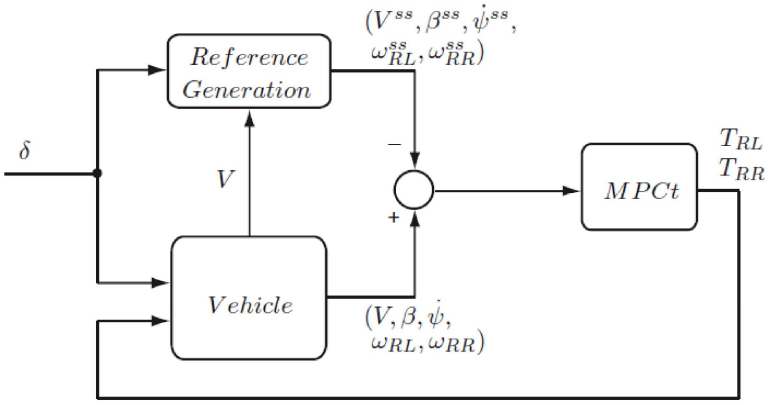

Figure 2.5: MPCt control structure

The second controller is the *MPCs* that neglects wheel dynamics, which allows for a simpler internal model that only includes the vehicle velocity, sideslip angle and yaw rate as states and uses rear wheel slips as input to calculate the torques. A sliding mode slip controller is added to calculate the torque demand on the two motors according to the longitudinal slip requests.

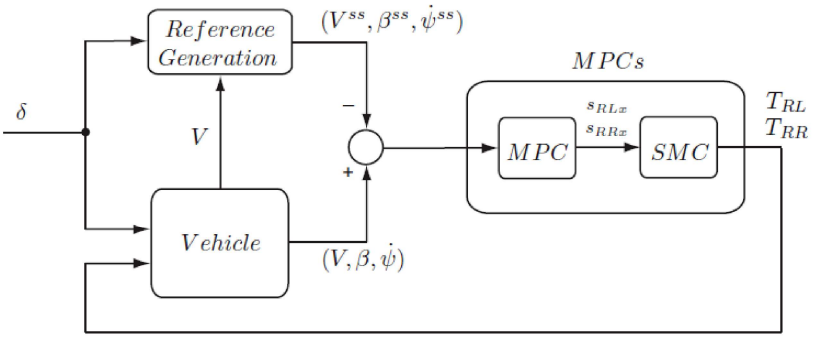

Figure 2.6: MPCs control structure

The results in [12] show that the MPC controller is able to achieve a lower sideslip angle and yaw rate compared to the LQR controller, whilst keeping the longitudinal slips within the bounds. Additionaly, the inclusion of wheel dynamics in *MPCt* formulation makes the optimization problem more computationally complex and requires faster sampling times whilst having no advantage in performance over the *MPCs*.

The MPC TV control strategy was also compared with a LQR controller and an uncontrolled vehicle through a u-turn and double lane change manoeuvre with varying friction levels in [14]. The vehicle that used MPC was stable in all manoeuvres, whereas the uncontrolled vehicle and the LQR controlled vehicle lost control during the double lane change manouevre. The MPC controlled vehicle also had the highest exit velocity while keeping the torque requests within the torque constraints.

2.5. NMPC Torque Vectoring

Instead of linearising the vehicle model, a nonlinear model predictive control formulation can also be used. The benefit of this is that the torque allocation is also taken into account in the top level controller and can be based on the objectives and constraints. One example of a NMPC scheme can be seen in figure 2.7. From the vehicle model, the steering angle, reference longitudinal forces and parameter vector Θ are given. With this information the reference yaw rate can be calculated, which is then sent to the NMPC TV control algorithm. Here, everything is determined to formulate the optimal control problem. This includes the nonlinear internal model, constraints, cost function weights and more, depending on what the designer wants to include. After the nonlinear optimal control problem is solved, the torques are then sent to the vehicle.

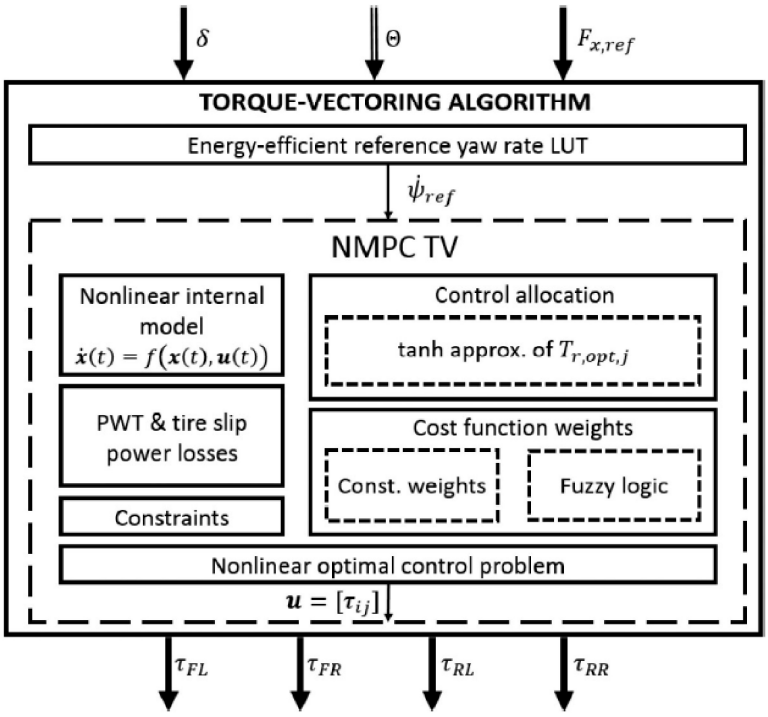

Figure 2.7: Scheme of NMPC TV Control [15]

In general the NMPC control law minimises a cost function *J*, with appropriate equality and inequality constraints. The optimal control problem is defined in discrete time in (2.11), where $\ell_n(\mathbf{x}(N))$ is the terminal cost, with N being the number of steps of the prediction horizon. $\ell(\mathbf{x}(k), \mathbf{u}(k))$ is the stage cost of the function, which for the nonlinear MPC is a nonlinear function. $\mathbf{x}$ and $\bar{\mathbf{x}}$ are the upper and lower limits for the states $\mathbf{x}$ and $\mathbf{u}$ and $\bar{\mathbf{u}}$ are the the upper and lower limits for the inputs $\mathbf{u}$. The discrete model is $\mathbf{x}(k+1) = f_d(\mathbf{x}(k), \mathbf{u}(k))$.

$$\min_{\mathbf{u}} J(\mathbf{x}(0), \mathbf{u}(\cdot)) := \ell_n(\mathbf{x}(N)) + \sum_{k=0}^{N-1} \ell(\mathbf{x}(k), \mathbf{u}(k)) \tag{2.11}$$

$$\begin{aligned} &s.t. \\ &\mathbf{x}(0) = \mathbf{x}_{in} \\ &\mathbf{x}(k+1) = f_d(\mathbf{x}(k), \mathbf{u}(k)) \\ &\mathbf{x} \leq \mathbf{x}(k) \leq \bar{\mathbf{x}} \\ &\mathbf{x} \leq \mathbf{x}(N) \leq \bar{\mathbf{x}} \\ &\mathbf{u} \leq \mathbf{u}(k) \leq \bar{\mathbf{u}} \\ &\mathbf{u}(\cdot) : [0, N-1] \end{aligned}$$

The way that TV is implemented with NMPC differs in the literature. In [15] the NMPC TV controller includes energy optimisation in the top-level controller, as understeer has an effect on the energy usage of the vehicle. The controller tracks the longitudinal, yaw rate, rear slip angle, powertrain loss, tyre power losses and the rear-to-total torque distribution. The stage cost of the NMPC is given in (3.26) defined as a least-squares function, and the constraints are given in [15].

$$\ell(x(k),u(k)) = W_{u,F_x} e_{F_x}^2 + W_{u,\dot{\psi}} e_{\dot{\psi}}^2 + + W_{u,PWT} P_{Loss,PWT}^2 + W_{u,Tyre} P_{Loss,Tyre}^2 + W_{u,LD}(e_{T_{r,left}}^2 + e_{T_{r,right}}^2) \quad (2.12)$$

The longitudinal force error is given by (2.13) where $F_{x,ref}$ is the total force demand from the drivability controller.

$$e_{F_x} = F_{x,ref} - [F_{x,FL} + F_{x,FR} + F_{x,RL} + F_{x,RR}] \quad (2.13)$$

The yaw rate error is given by:

$$e_{\dot{\psi}} = \dot{\psi}_{ref} - \dot{\psi} \quad (2.14)$$

The tyre slip power losses are the power losses through both the longitudinal and lateral slip and is given by:

$$P_{Loss,Tyre} = P_{Loss,Tyre,Long} + P_{Loss,Tyre,Lat} \quad (2.15)$$

The rear-to-total torque distribution for both sides is given in (3.28) with the reference $T_{r,ref,j}$ being determined in [15].

$$\begin{aligned} e_{T_{r,left}} &= \frac{\tau_{RL}}{\tau_{FL} + \tau_{RL}} - T_{r,ref,L} \\ e_{T_{r,right}} &= \frac{\tau_{RR}}{\tau_{FR} + \tau_{RR}} - T_{r,ref,R} \end{aligned} \quad (2.16)$$

The cost function weights given in (3.26) all have a different range, which is why each weight will be expressed as a ratio of a weighing coefficient ($r_{u,F_x}, r_{u,\dot{\psi}}, r_{u,\alpha_R}, r_{u,PWT}, r_{u,Tyre}, r_{u,LD}$) to the square of the corresponding scaling factor coefficient (U_{sc}^2), that represents the maximum expected value of the respective cost function variable. For example $W_{u,F_x} = \frac{r_{u,F_x}}{U_{sc,F_x}^2}$.

The weights are adjusted for the yaw rate error and the energy efficiency of the powertrain using a fuzzy controller. This allows the NMPC to be flexible for different scenarios as it can prioritise in energy efficiency during normal driving and yaw rate tracking in critical conditions. Based on this information the rules for the fuzzy controller can be established and is given in figure 2.8, where the weights will be defined by a combination of absolute yaw rate error and absolute sideslip angle.

EO=Energy Oriented *YR=Yaw Rate Tracking* *BW=Balanced Weights*		$\lvert e_{\dot{\psi}} \rvert$		
		Low	Medium	High
$\lvert\beta\rvert$	Low	EO	BW	YR
	Medium	EO	BW	YR
	High	EO	YR	YR

Figure 2.8: Adopted fuzzy rules

Now that it is known what type of tracking is required depending of the scenario, the cost function weighing coefficients relating to each scenario is given in figure 2.9

	Yaw Rate Tracking	Energy Oriented	Balanced Weights
r_{u,F_x}	2.5	2.5	2.5
$r_{u,\dot{\psi}}$	5	1	3
$r_{u,\alpha}$	1.5	1.5	1.5
$r_{u,PWT}$	1	5	2.5
$r_{u,Tire}$	1	5	2.5
$r_{u,LD}$	2.5	2.5	2.5

Figure 2.9: Cost Function Weighting Coefficients

With the cost function weights being given, the NMPC TV controller has all information necessary to function. The results show that the controller that had the adaptive cost function weights was able to outperform the controller with constant cost function weights in terms of responsiveness, stability, as well as increasing the energy efficiency of the vehicle.

Another benefit of the NMPC controller is that it has the ability to handle more complex systems, which is beneficial if TV were to be combined with other systems. This is done in [16], where the NMPC TV is combined with active suspension and aerodynamics are taken into account. The paper focuses on the integrated and optimal model based control of the wheel torque and anti-roll moment distributions. Therefore the anti-roll moment distribution is added in the cost function in addition to yaw rate tracking and the energy consumption. This is depicted in the TV and anti-roll moment distribution block in figure 2.10, where the outputs are the torques T_j,which are sent to the brake blending block and the front-to-total anti-roll moment distribution factor *f*, which is sent to the suspension force distribution block, where the active suspension forces $F_{act,j}$ are sent to the vehicle model.

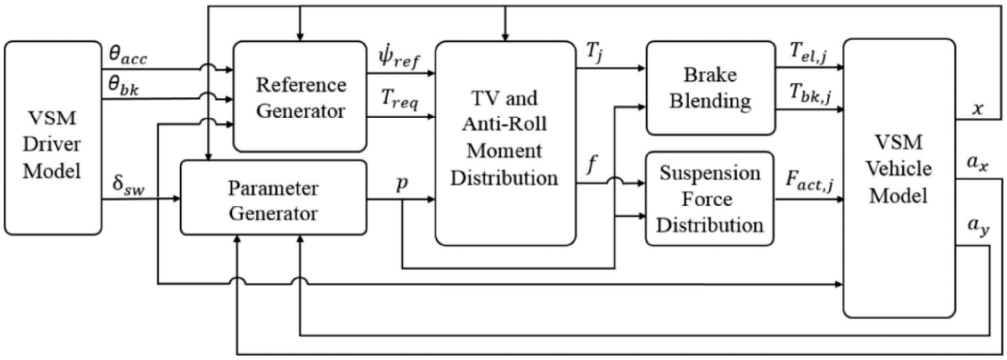

Figure 2.10: Scheme of NMPC TV Control with active suspension [16]

This controller was then compared to a PI controller and a NMPC controller that does not focus on energy consumption. The result of this comparison is that the power losses were decreased compared to the NMPC controller that does not focus on energy consumption, whilst the lateral load transfer was limited, the yaw rate error decreased and the exit speed increased. Compared to the PI controller the NMPC TV controller was more accurate in tracking the yaw rate reference, whilst decreasing the sideslip angle required for the manoeuvre, which enhances stability.

2.6. Summary

In this chapter the findings from literature are introduced. This started with an explanation about torque vectoring and its impact on vehicle stability. With its ability to design per-wheel motors, the controller is able to supply the power to each wheel directly, resulting in improved lateral performance, responsiveness, and stability. TV also enhances steering response, making the vehicle more agile and reducing undesired yaw rate response and body motion.

Then, the concept of path following was introduced, where different have been developed and tested for different driving scenarios and conditions. The use of torque vectoring in path following has also been investigated and shown to improve vehicle performance and agility, whilst being able to still follow the path. Another benefit was that an optimisation-based controller had more degrees of freedom in designing the cost function and tuning the weighting matrices.

Furthermore, model predictive control was explained and its suitability to use for torque vectoring was discussed. The benefit of using MPC for TV was because of the ability to take torque limits into account, while using current state measurements, state predictions and satisfying constraints on states and control inputs. Research also has shown that the MPC controller was able to outperform an LQR controller when it came to vehicle stability and satisfying constraints.

Finally, nonlinear model predictive control was introduced. The advantage of nonlinear model predictive control is that because it is able to work with a nonlinear vehicle model, that it can handle more complex systems, such as systems with adaptive cost function weights, or combining multiple systems into one controller, such as torque vectoring and active suspension. As a result, for this thesis the choice is to use nonlinear model predictive control for torque vectoring. In the next chapter, the design of the controller will be introduced.

3

Nonlinear Model Predictive Controller for Torque Vectoring

In this chapter, the controller design of the nonlinear model predictive controller for torque vectoring will be shown. At first, the control structure is depicted and the framework of the simulation is elaborated. Then, the internal model formulation is introduced and the vehicle and tyre model are explained. Furthermore, the optimal control problem is formulated in terms of the cost function, constraints and the controller implementation. Finally, the generation of the yaw rate reference is described.

3.1. Control Structure

The framework of the simulation, shown in figure 3.1, consists of:

- The NMPC TV block, shown in figure 3.2, where the nonlinear internal model $\dot{x}(t) = f(x(t), u(t))$, shown in section 3.2, with constraints, shown in section 3.3.2, and cost function, shown in section 3.3.1, is put into a nonlinear OCP. This is where the torques are generated (denoted by *T*) and then sent to the vehicle model.
- The vehicle model, which is applied through the CarMaker model in Simulink. Here the torques generated by the NMPC TV controller are sent to the model and then sends the variables needed for the nonlinear internal model to the online data block.
- The driver model, which generates the steering wheel angle either through Carmaker/Simulink and sends it to both the reference generator and the online data block.
- The reference generator, shown in section 3.4, where the steering angle δ and the longitudinal velocity are given as input and the yaw rate reference $\dot{\psi}_{ref}$ is generated and sent to the TV controller as a reference value.
- The online data block, which are the parameters that are needed for the nonlinear internal model, which are generated from the vehicle model and driver model. These parameters, denoted by parameter block Θ, are the steering wheel angle, the longitudinal and lateral accelerations, a_x and a_y, the velocity of the vehicle *V* and the sideslip angle β.

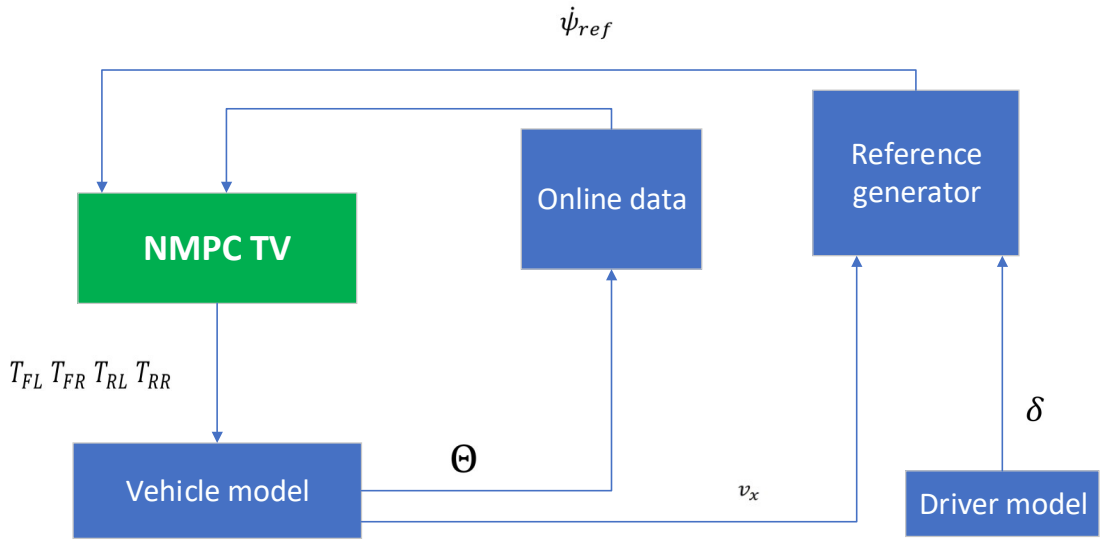

Figure 3.1: Block diagram overview of Simulink workflow

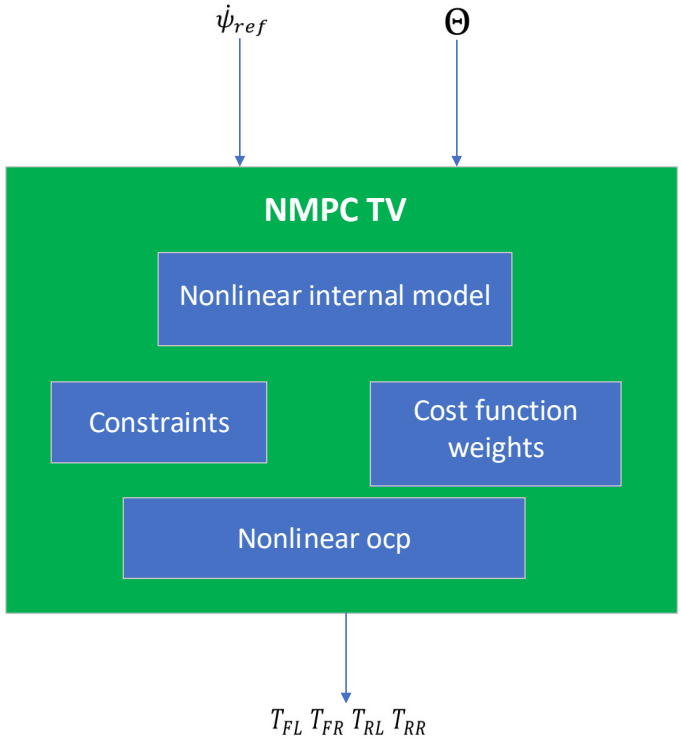

Figure 3.2: Contents of the nonlinear model predictive controller

3.2. Internal Model Formulation

The internal NMPC model is expressed through the continuous time formulation and given below:

$$\dot{x}(t) = f(x(t), u(t)) \tag{3.1}$$

with the state vector x being given as:

$$x = [\dot{\psi}\ \omega_{FL}\ \omega_{FR}\ \omega_{RL}\ \omega_{RR}] \tag{3.2}$$

where $\dot{\psi}$ is the yaw rate and ω_{ij} is the rotational velocity of the wheel, where subscript *i* = *F,R* denotes the front and rear axles and subscript *j* = *L,R* denotes the left and right side of the vehicle.

The control inputs are given in 3.3, where T_{ij} is the wheel torque.

$$u = [T_{FL}\ T_{FR}\ T_{RL}\ T_{RR}] \tag{3.3}$$

The parameter block , that is described in Section 3.1, is denoted by Θ and is formulated below:

$$\Theta = [\delta\ V\ a_x\ a_y\ \beta] \tag{3.4}$$

The prediction model formulation is described by the moment balance equations (3.5) and (3.6).

Yaw moment balance:

$$\begin{aligned}\ddot{\psi} =& \frac{1}{I_{zz}} l_f[(F_{x,FL} + F_{x,FR}sin(\delta)) + (F_{y,FL} + F_{y,FR}cos(\delta))] - l_r[F_{y,FL} + F_{y,FR}] \\ &+ \frac{t_w}{2}[(F_{x,FR} - F_{x,FL}cos(\delta) + (F_{y,FL} - F_{y,FR}sin(\delta) - F_{x,RL} + F_{x,RR}]\end{aligned} \tag{3.5}$$

where I_{zz} is the moment of inertia around the z-axis, l_f and l_r are the distance from the front and rear axis to the vehicle CoG respectively and t_w is the vehicle track width.

Wheel moment balance:

$$\dot{\omega}_j = \frac{1}{I_\omega} T_j - F_{x,j} R \tag{3.6}$$

where I_ω is the wheel moment of inertia, T_{ij} is the wheel torque and *R* is the effective wheel radius. The subscript *j* denotes the tyre where 1 is the front left, 2 the front right, 3 the rear left and 4 the rear right.

The aerodynamic drag and rolling resistance of the tyre are neglected as they are not affected by the distribution of the wheel torque.

3.2.1. Tyre Model

The longitudinal and lateral tyre forces, $F_{x,j}$ and $F_{x,j}$ are calculated through a simplified version of Pacejka's magic formula, as is done in [16]. The tyre forces are calculated as follows:

$$F_{x,j} = \frac{s_{x,j}}{s_j} \mu_{x0,j} F_{z,j} \tag{3.7}$$

$$F_{y,j} = \frac{s_{y,j}}{s_j} \mu_{y0,j} F_{z,j} \tag{3.8}$$

with $\mu_{x0,j}$ and $\mu_{y0,j}$ being given as:

$$\mu_{x0,j} = D_x sin(C_x arctan(B_x s_j) \tag{3.9}$$

$$\mu_{y0,j} = D_y sin(C_y arctan(B_y s_j) \tag{3.10}$$

where the tyre parameters are B, which is the cornering stiffness, C is the shape factor that controls the stretching along the x-axis and D is the peak value of the tyre force.

The combined theoretical slip s_j is given by:

$$s_j = \sqrt{s_{x,j}^2 + s_{y,j}^2} \tag{3.11}$$

with $s_{x,j}$ and $s_{y,j}$ being the longitudinal and lateral slip respectively and described by:

$$s_{x,j} = \frac{\sigma_j}{1 + \sigma_j} \tag{3.12}$$

$$s_{y,j} = -\frac{tan(\alpha_j)}{1 + \sigma_j} \tag{3.13}$$

3.2.2. Vehicle model

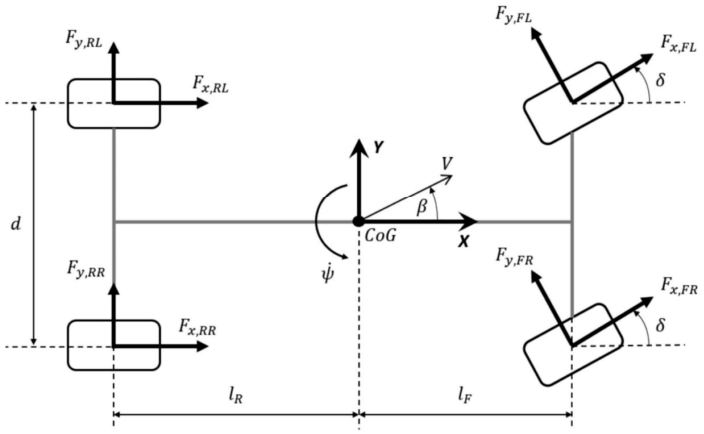

Figure 3.3: Top view of the planar model of the vehicle with indication of main variables [15]

The vehicle model that is used, is based on the planar model with the sign conventions given in figure 3.3. The advantage of this model is that it allows the use of a four-wheel drive system, with each motor regulating the torque of each wheel. This model is a modified version of the vehicle model in Dalboni's paper [16]. The main difference with Dalboni's paper is that a passive suspension will be used in this thesis, compared to the active suspension used in the paper. This means that the moments with regards to the active suspension are not applicable here.

Now, in order to determine the longitudinal and lateral forces, the longitudinal slip σ_j, the lateral slip angle α_j and the vertical force F_z are required.

The longitudinal slip ratio σ_j and slip angle α_j are formulated by:

$$\sigma_j = -\frac{v_{x,slip,j}}{v_{x,j}} \tag{3.14}$$

$$\alpha_j = arctan(\frac{v_{y,slip,j}}{v_{x,j}}) \tag{3.15}$$

with the longitudinal $v_{v_{x,slip,j}}$ and lateral slip velocities $v_{y,slip,j}$ being:

$$v_{x,slip,j} = v_{x,j} - \omega_j R \tag{3.16}$$

$$v_{y,slip,j} = v_{y,j} \tag{3.17}$$

where $v_{x,j}$ and $v_{y,j}$ are the longitudinal and lateral velocities of the wheel hubs and expressed in the wheel reference frame given by equations (3.18) - (3.21).

for j = 1,2:

$$v_{x,j} = cos(\delta_j)[Vcos(\beta) + (-1)^j \frac{t_w}{2}\dot{\psi}] + sin(\delta)[Vsin(\beta) + l_f\dot{\psi}] \tag{3.18}$$

$$v_{y,j} = -sin(\delta_j)[Vcos(\beta) + (-1)^j \frac{t_w}{2}\dot{\psi}] + cos(\delta)[Vsin(\beta) + l_f\dot{\psi}] \tag{3.19}$$

and for j= 3,4:

$$v_{x,j} = Vcos(\beta) + (-1)^j \frac{t_w}{2}\dot{\psi} \tag{3.20}$$

$$v_{y,j} = Vsin(\beta) + l_r\dot{\psi} \tag{3.21}$$

The vertical tyre forces $F_{z,j}$ in (3.7) and (3.8) are expressed as:
for j = 1,2:

$$F_{z,j} = \frac{1}{2}mg\frac{l_r}{L} - \Delta F_z^x + (-1)^j \Delta F_{z,F}^y \tag{3.22}$$

for j = 3,4:

$$F_{z,j} = \frac{1}{2}mg\frac{l_f}{L} - \Delta F_z^x + (-1)^j \Delta F_{z,R}^y \tag{3.23}$$

with the longitudinal load transfer ΔF_z^x being given by:

$$\Delta F_z^x = \frac{1}{2}ma_x\frac{h_{CG}}{L} \tag{3.24}$$

where h_{CG} is the height of the CoG. The lateral load transfer ΔF_z^y is given in 3.25, with h_{roll} being the roll centre height.

i = front,rear

$$\Delta F_{z,i}^y = \frac{ma_y h_{roll,i}}{Lt_w} \tag{3.25}$$

3.3. Optimal Control Problem Formulation

3.3.1. Cost function

With the optimal control problem being defined in (2.11), the stage cost of the NMPC is given in (3.26) defined as a least-squares function.

$$\ell(x(k),u(k)) = W_{u,\dot{\psi}} e_{\dot{\psi}}^2 + W_{u,\Delta T_L}(\Delta T_L)^2 + W_{u,\Delta T_R}(\Delta T_R)^2 + W_{u,T_{tot}}(T_{tot})^2 \tag{3.26}$$

The yaw rate error cost, that is set to track the yaw rate reference, is given by:

$$e_{\dot{\psi}} = \dot{\psi}_{ref} - \dot{\psi} \tag{3.27}$$

The front-to-total torque distribution for both vehicle sides is given in (3.28), where $f_{T,L,opt}$ and $f_{T,R,opt}$ are the reference front-to-total torque distribution coefficients.

$$\begin{aligned} \Delta T_{f,L} &= |[f_{T,L,opt} - 1]T_{el,1} + f_{T,L,opt}T_{el,3}| \\ \Delta T_{f,R} &= |[f_{T,R,opt} - 1]T_{el,2} + f_{T,R,opt}T_{el,4}| \end{aligned} \tag{3.28}$$

The total torque cost that is set to reduce the amount of total torque being sent to the wheels, is given by:

$$\Delta T_{tot} = \sum_{j=1}^{4} T_j \tag{3.29}$$

$W_{u,\dot{\psi}}$, $W_{u,\Delta T_L}$, $W_{u,\Delta T_R}$ and $W_{u,T_{tot}}$ are the cost function weights of the yaw rate, the front-to-total motor torque distribution on the left hand side, the front-to-total motor torque distribution on the right hand side and the total torque respectively. The values of these weights are given in appendix B.

3.3.2. Constraints

The constraints that are shown in this subsection will be used for all of the controllers. The additional constraints for the path following controllers will appear in section 4.3.2. These baseline constraints are set as such in order to limit the maximum values of the control outputs, to ensure vehicle and controller stability. The constraints for the TV controller are shown below:

$$|\dot{\psi}| = \frac{\mu g}{V} \tag{3.30}$$

$$|T_{ij}| \leq 500Nm \tag{3.31}$$

$$|\delta| \leq \frac{360}{180\pi SR} \tag{3.32}$$

The yaw rate constraint (3.30) limits the yaw rate depending on the tyre-road friction coefficient μ and the velocity of the vehicle *V*, where the value for the bounds was set in [15]. As there is no information on the motor limits in the form of its static torque map an additional constraint is added the torques of each wheel in (3.31) in order to avoid excessive torque requests.
The steering wheel angle is constrained by (3.32), with *SR* being the steering ratio.

3.3.3. Controller Implementation

The NMPC algorithm was set up using the ACADO toolkit, which is able to run the NMPC with constraints swiftly. The Gauss-Newton method with a Hessian approximation is chosen as an algorithm because of its ability to find an optimal value if the initial guess is close enough. To increase the likelihood of finding a good initial guess, multiple shooting is used for discretisation. In order to avoid numerical problems related with the inversion of the Hessian matrix, a Levenberg-Marquardt regularsation value is introduced and set to 10^{-4}.
The fourth order Runge-Kutta inegrator is selected as the integrator with the number of integration steps set to $3N_p$, in order to reduce the complexity of the optimisation problem. The prediction horizon is set to $N_p = 6$ and the sampling time $T_s = 0.01$s, as the cost of the optimisation does not improve by increasing the prediction time. Furthermore, the solver that is used is the QPOASES 3 QP solver and the sparse QP solution is set to full condensing N2.

3.4. Yaw rate Reference

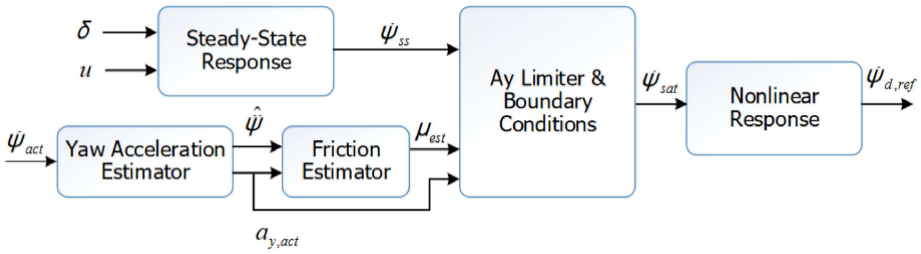

Figure 3.4: Yaw rate reference generation scheme

In order to establish yaw moment control, a yaw rate reference needs to be generated. The general scheme of how the yaw rate is generated is depicted in figure 3.4. Here, the steady-state response defines the desired steady-state yaw rate, which is calculated based on a linear bicycle model:

$$\dot{\psi}_{ss,\delta} = G_{yaw}^{ss}\delta \tag{3.33}$$

With the steady-state yaw rate gain given by:

$$G_{yaw,\delta}^{ss} = \frac{u}{L_w + \frac{K_{us}u^2}{g}} \tag{3.34}$$

where the inputs are the longitudinal velocity u, the wheelbase L, the understeer gradient K_{us} and the gravitational constant g. The linear bicycle model in only valid below 4 m/s^2 at high friction conditions. Therefore, the steady-state response cannot be used directly.

Next, there is the friction estimator, which evaluates the friction and constrains the desired steady-state response. The estimated friction is dependent on utilised, yaw rate-based and predefined high friction using rule-based logic.

As the steady-state yaw rate, estimated friction and the estimated lateral acceleration are now given, a block is created to limit the lateral acceleration and set boundary conditions to saturate the yaw rate. The ay limiter should reduce the steady-state yaw rate at the higher levels of lateral acceleration according to the available friction level. The yaw rate reference model is tuned for high friction conditions. For low friction conditions, the set-point is scaled down using the lateral acceleration. Like the lateral acceleration, the maximum reference yaw rate should be limited by the available friction level.

The saturated steady-state response is not described in the dynamic vehicle response. Taking the yaw frequency ω, the yaw damping ratio ζ and yaw delay $\omega_{n,0}$ into account, the yaw rate response becomes:

$$\dot{\psi}_{ref} = G_{yaw}^{ss,\delta} \frac{1 + \frac{ml_f u}{LC_{ar}} j\omega}{1 + 2\zeta(\frac{j\omega_n}{\omega_{n,0}}) - (\frac{\omega_n}{\omega_{n,0}})^2} \delta \tag{3.35}$$

where the inputs are the steady-state yaw rate gain, given in (3.34), the vehicle mass m, the distance between the front axle and the horizontal centre of gravity (CoG) position of the vehicle l_f and the rear cornering stiffness $C_{\alpha r}$.

3.5. Summary

The chapter discusses the design of a Nonlinear Model Predictive Controller (NMPC) for torque vectoring in a vehicle. This was done by depicting the control structure, which contained the NMPC TV control structure and the schematic of the Simulink workflow. The parts of the NMPC TV structure were then expanded upon by showing the nonlinear internal model, with the state vector including the yaw rate and rotational velocity of each wheel. A simplified formula of Pacejka's magic formula was used for the tyre model which generates the longitudinal and lateral tyre forces. The planar model was chosen as the vehicle model in order to use a four-wheel drive system where each motor torque of each wheel is regulated

Furthermore, the optimal control problem was formulated with a cost function that includes the yaw rate error, front-to-total torque distribution for both wheels and the total torque. Some constraints were then created in order to ensure both vehicle and controller stability. The constraints limit the maximum amount of yaw rate, the wheel torque and the wheel angle. Finally, the yaw rate reference was generated where the steady-state yaw rate gain, which is dependent on the understeer gradient, and the steering wheel angle were given as inputs. As nonlinear model predictive control allows for more design freedom, it is also possible to make a formulation that includes both torque vectoring and path following. The controller design for this will be introduced in the next chapter.

4

Path Following with Nonlinear Model Predictive Control

For this chapter, the controller design of the nonlinear model predictive controller that now implements both torque vectoring and path following will be shown. First, the control structure is shown and the framework of the simulation will be elaborated. Then, the internal model formulation with the cost function and constraints are given. Finally, the yaw rate reference generation that is derived from the added yaw moment from torque vectoring is introduced.

4.1. Control structure

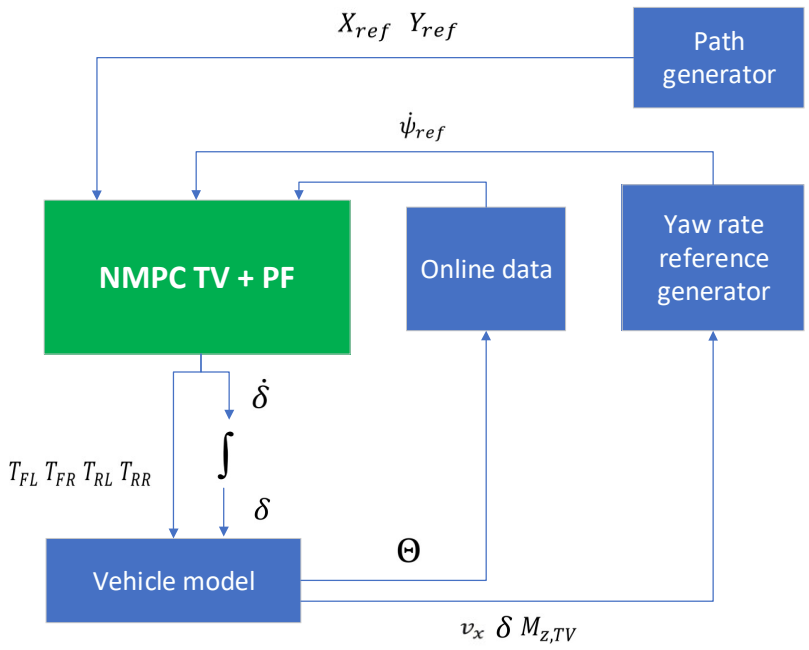

Figure 4.1: Block diagram overview of Simulink workflow

The framework of the simulation, shown in figure 4.1 now consists of:

- The NMPC TV + PF block, where the nonlinear internal model now also includes the states necessary to perform path following in section 4.2, with a cost function that includes costs for torque vectoring and path following in section 4.3.1 and constraints from section 3.3.2 and section 4.3.2, which are all put in a nonlinear OCP. As a result the torques (denoted by *T*) and the steering rate $\dot{\delta}$ are generated and sent to the vehicle model.
- The vehicle model, which receives the torques from the NMPC controller and the steering angle, which is integrated from the steering rate. It then sends the relevant parameters to the online data block (denoted by Θ) and the necessary parameters to the yaw rate reference generator. The vehicle model is a created model in Simulink and can be found in appendix D.
- The yaw rate reference generator (shown in section 4.4), where the steering angle, the longitudinal velocity and the moment added by torque vectoring ($M_{z,TV}$) are given as input and the yaw rate reference $\dot{\psi}_{ref}$ is generated and sent to the NMPC controller.
- The path generator, which generates a reference path given by x and y coordinates to the NMPC controller. The manoeuvres that will generate the reference paths will be depicted in chapter 6.

4.2. Internal Model Formulation

With the internal model formulation being given in (3.1), the state vector x is now changed to accommodate path following as follows:

$$x = [\delta\ \psi\ \dot{\psi}\ X_p\ Y_p\ \omega_{FL}\ \omega_{FR}\ \omega_{RL}\ \omega_{RR}] \tag{4.1}$$

where ψ is the yaw angle, which is added to keep track of the vehicle heading and X_p and Y_p are the longitudinal and lateral positions respectively, as it is now important to track the position of the vehicle. The steering wheel angle is also added as a state because it is important to track the wheel angle for PF.

For the control inputs given in (4.2), the steering rate $\dot{\delta}$ is also added.

$$u = [T_{FL}\ T_{FR}\ T_{RL}\ T_{RR}\ \dot{\delta}] \tag{4.2}$$

The parameter block Θ, now does not include the steering angle as that is now a state.

$$\Theta = [V\ a_x\ a_y\ \beta] \tag{4.3}$$

The prediction model formulation includes equations 3.5 and 3.6 in addition to the formulations for both the change in longitudinal and lateral positions, the yaw rate and the steering rate that are given below:

$$\dot{X}_p = v_x \cos\psi - v_y \sin\psi \tag{4.4}$$

$$\dot{Y}_p = v_x \sin\psi + v_y \cos\psi \tag{4.5}$$

$$\dot{\psi} = \dot{\psi} \tag{4.6}$$

$$\dot{\delta} = \dot{\delta} \tag{4.7}$$

4.3. Optimal Control Problem Formulation

4.3.1. Cost function

As the controller now has to also account for path following, some additional terms have been added for the stage cost in (4.8) compared to (3.26), with the new terms being explained below:

$$\ell(x(k),u(k)) = W_{u,\dot{\psi}} e_{\dot{\psi}}^2 + W_{u,\Delta T_L}(\Delta T_L)^2 + W_{u,\Delta T_R}(\Delta T_R)^2 + W_{u,\Delta T_{tot}}(\Delta T_{tot})^2 + W_{u,Y_p} e_{Y_p}^2 + W_{u,\dot{\delta}} \dot{\delta}^2 \quad (4.8)$$

As the aim with path following is to follow the reference path, there is a need for a cost to track lateral (Y_p) position, as the manoeuvre requires the vehicle to only move its lateral position. This is done by trying reduce the lateral error between the reference path and the actual path in (4.9). Additionally, there is also a set cost on the steering rate as with torque vectoring, there is less steering angle needed.

$$e_Y = Y_{ref} - Y_p \quad (4.9)$$

W_{u,Y_p} and $W_{u,\dot{\delta}}$ are the cost function weights of the lateral position and the steering rate respectively.

In this research multiple formulations of this cost function will be compared to each, which is listed as follows:

1. One formulation that performs the path following manoeuvre without using torque vectoring. This is done by constraining the wheel torques to give zero input, ensuring that the only control input is the steering rate.
2. Another formulation that performs the path following manoeuvre by using only torque vectoring and therefore no steering angle. This is done by constraining the steering rate to give zero input, ensuring that the wheel torques are only control inputs.
3. A formulation that performs the path following manoeuvre by using both the steering angle and torque vectoring. This means that both the wheel torques and the steering rate will be used as control inputs.

The prediction horizon of all the control formulations above were set to $N_p = 30$, with the rest of the controller settings being the same as in section 3.3.3.

4.3.2. Constraints

Now that the steering rate is also an input, there is now a constraint set on the steering rate in (4.10), as there is a limitation on how fast the steering angle can change.

$$|\dot{\delta}| \leq \frac{800}{180\pi SR} \quad (4.10)$$

To ensure that the torques always go in the right direction, additional constraints (4.11) and (4.12) were created. These constraints ensure that with a positive lateral acceleration, the wheel torques on the right side of the vehicle (T_{right}) are positive and the torques on the left side of the vehicle (T_{left}) are negative and the other way around when the lateral acceleration is negative.

$$a_y * T_{left} \leq 0 \quad (4.11)$$

$$a_y * T_{right} \geq 0 \quad (4.12)$$

4.4. Yaw rate reference

In section 3.4 the steady-state yaw rate reference is derived by using the bicycle model and solving the lateral force balance and moment balance around the z-axis. However, with the vehicle using TV, there is now a yaw moment that is added to the vehicle by TV. This is also depicted in figure 4.2, where the added yaw moment from torque vectoring is denoted by $M_{z,TV}$.

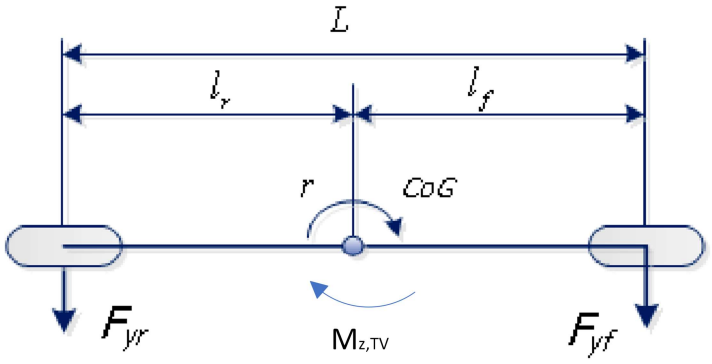

Figure 4.2: Bicycle model with added yaw moment from torque vectoring

With the moment balance around the z-axis, the lateral force balance and the steering law, the yaw rate reference can be derived, which is done in appendix C.1. The result of the steady-state yaw rate in terms of the added yaw moment from torque vectoring is given by:

$$\dot{\psi}_{ss,M_z} = G^{ss}_{yaw,Mz} M_{z,TV} \tag{4.13}$$

With the steady-state yaw rate gain being:

$$G^{ss}_{yaw,M_z} = \frac{(C_{\alpha f} + C_{\alpha r})u}{LC_{\alpha f}C_{\alpha r}(L + \frac{K_{us}u^2}{g})} \tag{4.14}$$

However, as the vehicle can also steer in combination with TV, the contribution from the steering angle also needs to be taken into account. The steady-state yaw rate derived from the steering angle that is given in section 3.4 is:

$$\dot{\psi}_{ss,\delta} = \frac{u}{L + \frac{K_{us}u^2}{g}}\delta \tag{4.15}$$

Now that the steady state yaw references derived from the yaw moment from TV and the steering angle are given, both can be combined in order to get the nonlinear yaw rate response, which looks as follows:

$$\dot{\psi}_{ref} = \frac{1 + \frac{ml_f u}{LC_{ar}} j\omega_n}{1 + 2\zeta(\frac{j\omega_n}{\omega_{n,0}}) - (\frac{\omega_n}{\omega_{n,0}})^2}(\dot{\psi}_{ss,\delta} + \dot{\psi}_{ss,M_z}) \tag{4.16}$$

4.5. Summary

The design of the nonlinear model predictive controller that included both torque vectoring and path following was introduced in this chapter. At first the control structure was shown and explained. Then, the internal model formulation was introduced, which now includes states and inputs to also accommodate for path following alongside torque vectoring as well as a revised prediction model formulation. Furthermore, the optimal control problem formulation is introduced, where the cost function, alongside the costs relevant for torque vectoring, now also includes costs to follow the path and to reduce the steering rate.

At last, a novel yaw rate reference generation is introduced, where the bicycle model now includes the yaw moment that is generated by torque vectoring. This yaw moment is now also included in the yaw rate reference alongside the yaw rate reference determined from the steering angle. As the novel controllers are now given, there are some benchmarks controllers required for comparison. These benchmark controllers will be introduced in the next chapter.

5

Benchmark TV controllers

The benchmark controllers for torque vectoring will be introduced in this chapter. At first the control structure for torque vectoring is introduced, which consists of a high level controller, which in this research will be the PD or LQR controller and the low level controller, which is the torque allocator. Next, the formulation for the benchmark controllers, which are the PD controller and the LQR controller, will be shown. At last, the formulation for the torque allocation will be elaborated.

5.1. Control structure

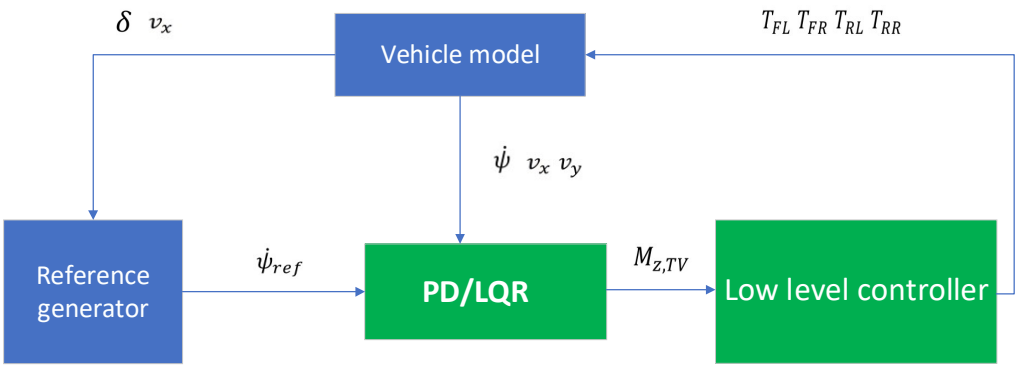

Figure 5.1: Block diagram overview of Simulink workflow for PD/LQR controller

The framework of the simulation consists of:

- The yaw rate reference generator, which generates the reference yaw rate based on the steering angle and the longitudinal velocity.
- The high level controller, which is either the PD or the LQR controller. The yaw rate error, which is the difference between the reference yaw rate $\dot{\psi}_{ref}$ and the measured yaw rate $\dot{\psi}$, is given as an input for both controllers. For the LQR controller, the longitudinal and lateral velocities are also given as inputs. Based on all of the information above the high level controller derives the required additional yaw moment to minimise the yaw rate error.
- The low level controller, which allocates the wheel torques based on the direction and magnitude of the yaw moment generated by the high level controller.
- The vehicle model which receives the wheel torques from the controller, then sends the measured quantities to the reference generator and the high level controller.

5.2. PD

One of the more widely-used strategies is proportional-integral-derivative (PID) control. This is a widely used feedback control mechanism, where the error between the reference and measured value is constantly calculated. There are multiple ways to apply PID control in torque vectoring. One way is by using PD control. Based on the yaw rate reference and the current yaw rate, the yaw rate error is calculated, which is used as an input for the controller. The controller consequently determines the total amount of yaw moment that needs to be added to the vehicle in order to get the desired yaw rate, which is implemented in the high level controller. The equation is given in 5.1, where $M_{z,TV}$ is the additional yaw moment.

$$M_{z,TV} = K_p(\dot{\psi}_{ref} - \dot{\psi}_{meas}) + K_d \frac{d}{dt}(\dot{\psi}_{ref} - \dot{\psi}_{meas}) \tag{5.1}$$

The gains for the PD controller are denoted by K_p, which is the proportional gain and K_d, which is the derivative gain. These gains were tuned to ensure good tracking of the yaw rate reference by reducing the yaw rate error and are given in table B.1 in the appendix.

5.3. LQR

Another controller that can be used for the yaw moment control is the linear quadratic regulator (LQR). LQR is used for linear systems, which is why the linear bicycle model is used as the vehicle model. The controller tries to minimise the error between the desired states and the current states denoted by x, where the states are the lateral velocity v_y and the yaw rate ψ. This is done by adapting the control input, which is the yaw moment M_z. Based on this information, the state update equation is given in (5.2).

$$\dot{x} = Ax + BM_z \tag{5.2}$$

With the following A and B matrices:

$$A = \begin{bmatrix} -\frac{C_{\alpha f}+C_{\alpha r}}{mu} & \frac{l_r C_{\alpha r}-l_f C_{\alpha f}}{mu} - u \\ \frac{l_r C_{\alpha r}-l_f C_{\alpha f}}{I_{zz} u} & -\frac{l_f^2 C_{\alpha f}+l_r^2 C_{\alpha r}}{I_{zz} u} \end{bmatrix}$$
$$B = \begin{bmatrix} 0 \\ I_{zz} \end{bmatrix} \tag{5.3}$$

where $C_{\alpha f}$ and $C_{\alpha r}$ are the cornering stiffnesses for the front axle and the rear axle respectively, m is the mass of the vehicle, u is the longitudinal velocity, l_f and l_r are the distance from the CoG to the front axle and rear axle respectively and I_{zz} is the moment of the body inertia around the z-axis.

In order to control the system weighting matrices are setup, where Q is the state weighting matrix, with a size of 2x2 and R is the input weight vector that is 1x1. The weights are tuned to ensure that high values of the yaw rate error are penalised to track the yaw rate reference and to penalise high lateral velocity to increase damping in the system while the amount of additional yaw moment input is reduced. The values of the weights are given in appendix B.

5.4. Torque Allocation

As the added yaw moment that is required to reduce the yaw rate error is now known, it is now time to convert it into wheel torques. One way of doing is, is by having the torque applied to all wheels be proportional to the vertical load on each wheel. The benefit of this strategy is that there is a smaller variation of the understeer gradient compared to having a torque distribution where only there is only a difference between the left and right wheels [17].
In order to obtain the wheel torques, the added yaw moment will be split into a fraction which is added to the front axle and a fraction which is added to the rear axle. These fractions are the added yaw moment for the front axle $M_{z,f}$ and the added yaw moment for the rear axle $M_{z,r}$. The values will be determined by the magnitude of the vertical tyre forces, which can be seen in (5.4) and in (5.5).

$$M_{z,f} = \frac{M_{z,total}(F_{z,FL} + F_{z,FR})}{F_{z,FL} + F_{z,FR} + F_{z,RL} + F_{z,RR}} \tag{5.4}$$

$$M_{z,r} = \frac{M_{z,total}(F_{z,RL} + F_{z,RR})}{F_{z,FL} + F_{z,FR} + F_{z,RL} + F_{z,RR}} \tag{5.5}$$

Based on the added yaw moment, the torques are then calculated in (5.6) and (5.7), where R is the effective wheel radius and t_w is the track width.

$$T_{f,i} = \frac{R}{t_w} M_{z,f} \tag{5.6}$$

where $i \in [FL, FR]$

$$T_{r,j} = \frac{R}{t_w} M_{z,r} \tag{5.7}$$

where $j \in [RL, RR]$

5.5. Summary

The benchmark controllers that will be used for the torque vectoring manoeuvres were introduced in this chapter.
At first, the control structure for the TV controllers was depicted and elaborated. Then, the PD controller was introduced by showing its formulation, which aims to decrease the yaw rate error by adding a yaw moment and the relevant controller gains were shown.
Next, the LQR controller was introduced by showing the state formulation. The aim is to reduce the yaw rate error and lateral velocity, with the added yaw moment being a changeable input. With the help of the weighting matrices these goals can be achieved.
At last, the torque allocation was explained. Here, the torques are calculated by having the applied torques be proportional to the vertical wheel load.
As all the controllers have now been introduced, the scenarios and key performance indicators will be set up to make a comparison between the controllers.

6

Evaluation methods

In order to find out compare the NMPC implementation with the benchmarks controllers from chapter 5, a few scenarios will be presented. Some scenarios are introduced to compare the controllers that have only the capability of performing torque vectoring and other scenarios are introduced to compare controllers that perform the path following manoeuvres. Then the key performance indicators, which are based on literature, will be used to put the vehicle performance into numbers.

6.1. Scenarios

6.1.1. Sine with Dwell

In order to compare the torque vectoring controllers with each other, it needs to be tested for vehicle stability. One manoeuvre that is used to test vehicle stability is the Sine with Dwell (SwD) test, according to the specifications in ISO 19365:2016 [18]. The manoeuvre is performed at a given entry velocity and starts with a predefined steering input, where the vehicle first turns left, then immediately goes right, where it stays at a consistent steering angle for 500 ms and at last the steering angle is returned to its center. This is also depicted in figure 6.1.

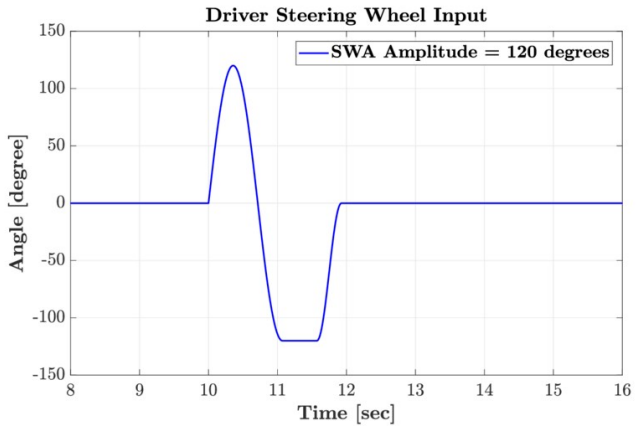

Figure 6.1: Steering angle plotted against time for the sine with dwell manoeuvre [19]

6.1.2. Double lane change

The double lane change (DLC) manoeuvre, also called an obstacle avoidance scenario, is one of the most common manoeuvres found in literature to perform path following. The aim is to navigate through a double-lane change, which is defined by three clusters of cones according to the specifications of ISO 3888-2:2011 [20]. The vehicle enters the course at a set velocity, then the throttle is released and the vehicle then tries to navigate the manoeuvre without hitting a cone.
For the path following controller a reference path is created, which the vehicle has to follow as accurately as possible. With this manoeuvre, the agility, responsiveness and tracking capabilities of the vehicle can all be tested.

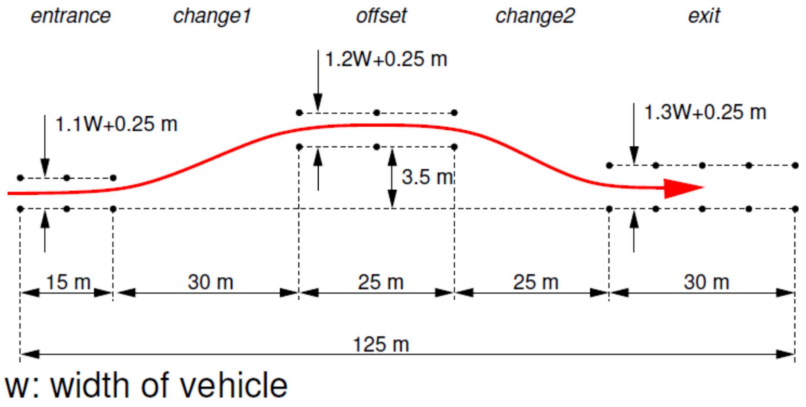

Figure 6.2: Double lane change trajectory

6.2. KPIs

The key performance indicators enumerates the effectiveness of the proposed controllers. The KPIs will be normalised with respect to the implementation which achieves the highest score by getting the lowest value (e.g. getting low steering effort would result in a high KPI value).

- $|\dot{\psi}_{max}|$: Peak absolute value of the yaw rate, in order to assess yaw rate effort. The higher this value is, the quicker the vehicle will rotate.
- $RMS(e_{\dot{\psi}})$: Root mean square value of the yaw rate error, which evaluates the yaw rate tracking performance.
- $|a_{y,max}|$: Peak absolute value of the lateral acceleration, in order to assess the lateral performance.
- $|\beta_{max}|$: Peak absolute value of the sideslip angle to assess how each vehicle utilised the tyre grip.
- $|T_{max}|$: Peak absolute value of the wheel torques, in order to compare the controller effort.
- $RMS(e_Y)$: Root mean square error of the lateral position, which evaluates the ability of the controller to follow the reference path.
- Normalised integral of the absolute value of the steering angle δ_{SW}:

$$IA_{\delta_{SW}} = \frac{1}{t_{fin} - t_{in}} \int_{t_{in}}^{t_{fin}} [\delta_{SW}] dt \tag{6.1}$$

  where t_{in} and t_{fin} are the initial and final times in the relevant part of the test, calculated when the EV enters and leaves the obstacle avoidance course. $IA_{\delta_{SW}}$ assesses the required steering effort to follow the reference path. In order to compare the steering effort during cornering, a condition has been formulated that the steering angle needs to be at least one degree.

6.3. Summary

The evaluation methods to compare all of the controllers were introduced in this chapter. This consists of scenarios and KPIs. The first scenario that was presented is the sine with dwell test, which is used to test the vehicle stability. Then, the double lane change manoeuvre was introduced, which can be used to compare both all torque vectoring controllers with each other for stability as well as the path following controllers in following the reference path.
Next, the KPIs were introduced in order to evaluate how each controller performs in terms of vehicle stability, handling, as well as following the reference path.

7

Results

The results for the different simulations will be shown in this chapter. At first, the different type of controllers that perform only torque vectoring will be compared to each other and a vehicle where no torque vectoring is applied. The manoeuvres that are used to compare the controllers are the sine with dwell test and the DLC. With the help of KPIs and figures, these controllers are compared against each other.
Then, the path following controllers that are described in section 4.3.1 are compared against each other in a DLC manoeuvre.

7.1. Torque Vectoring Controllers

7.1.1. Sine with dwell

Looking at the KPIs in table 7.1, it can be seen that all of the torque vectoring controllers outperform the vehicle without torque vectoring (No TV controller) in terms of increasing the maximum yaw rate, lateral acceleration and the utilisation of the the tyre by an increased sideslip angle. Apart from the NMPC, the TV controllers also outperform the controller without TV in terms of yaw rate tracking.

When comparing the TV controllers with each other, it can be seen that the maximum yaw rate and lateral acceleration is similar in table 7.1, with the NMPC controller getting the highest value. The overall yaw rate is also similar, though the PD and LQR controller maintain a higher yaw rate, when turning right as can be seen in figure 7.1. Looking at the KPI table, the PD controller has the best yaw rate tracking, followed by the LQR controller. However, figure 7.1 shows that the difference mainly is there during steady-state cornering, whereas at the points where the steering angle of the vehicle changes instantaneously, the yaw rate tracking of the NMPC controller is similar to the PD controller and better than the LQR controller. The LQR and NMPC controllers get a slightly better lateral acceleration compared to the PD controller and all of the controllers manage to have a higher lateral performance than the vehicle without torque vectoring.
Comparing the maximum sideslip angle it can be seen that the LQR controller uses the smallest sideslip angle to complete the manoeuvre, whereas the PD and NMPC controllers are quite similar. This shows that during this manoeuvre the LQR controller is quite efficient because it manages to get the highest lateral acceleration, by a small margin, with the lowest sideslip angle.

	$\dot{\psi}_{max}$ (deg/s)	RMS($e_{\dot{\psi}}$)(deg/s)	$a_{y,max}(m/s^2)$	$\beta_{max}(deg)$	$T_{max}(Nm)$
No TV	35.64	2.38	7.94	1.30	N/A
PD	40.29	1.56	8.18	1,78	434
LQR	40.45	1.97	8.25	1,66	271
NMPC	40.77	2.27	8.23	1.81	500

Table 7.1: Sine with Dwell results for V_{in} = 50 km/h

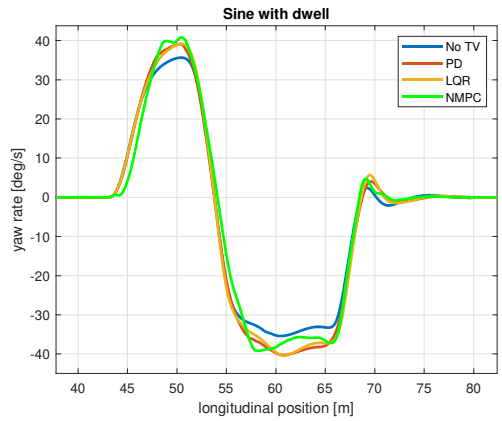

(a) Yaw rate of all controller

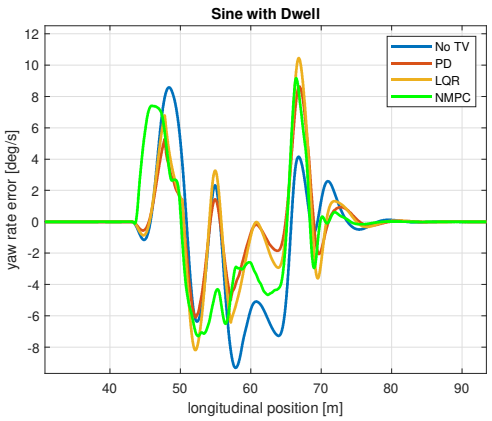

(b) Yaw rate error

Figure 7.1: Yaw rate plots of all the controllers

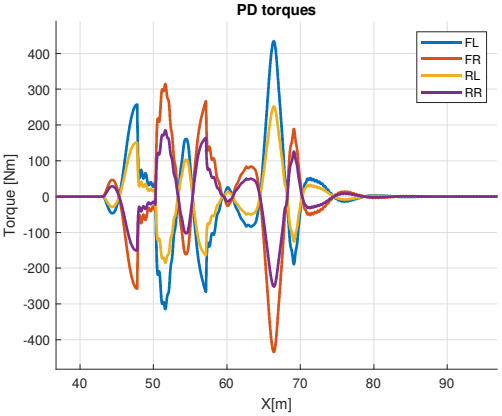

(a) Torques of the PD controller

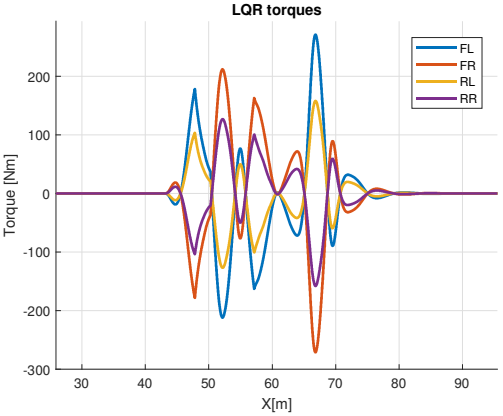

(b) Torques of the LQR controller

Figure 7.2: Plots of the torques for the various controllers

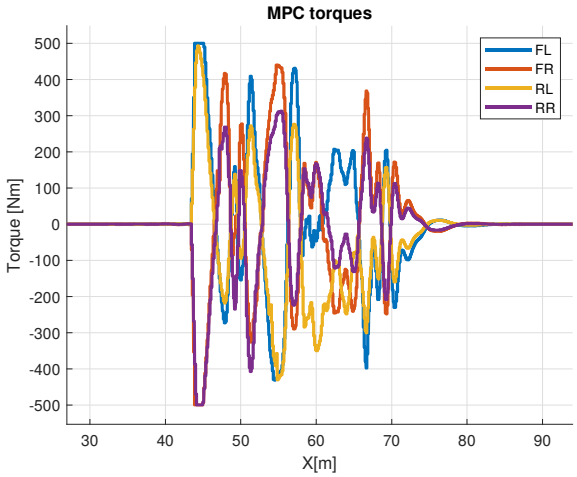

Figure 7.3: Torques from the MPC controller performing the sine with dwell manoeuvre

The torque plots of the PD and LQR controllers can be seen in figure 7.2. One observation that can be made is that the way that the torques are applied by the PD and LQR controllers is very similar. The key differences being that the torque application of the LQR controller appears slightly smoother

and that the PD controller requires higher torques to perform the manoeuvre. The only benefit the PD controller gets in return is better yaw rate tracking, whereas the LQR controller outperforms the PD controller in every other metric.

When comparing the NMPC controller in figure 7.3 to the LQR and PD controllers in figure 7.2, the first thing that is noticeable is that the NMPC controller uses higher torques throughout. The torques are high especially when turning in, afterwards the torques do not get higher than 425 Nm.
Another observation that can be made is that the MPC controller seems to constantly change the torque direction throughout the manoeuvre, until the steering angle returns to zero. This could not be corrected by changing the controller weights or by adding the constraints from 4.11 and 4.12, which resulted that the controller returned an infeasible solution.

7.1.2. Double lane change

The KPIs for the DLC manoeuvre are shown in table 7.2. The benchmark controllers are able to get a higher yaw rate and a better yaw rate tracking than the vehicle without TV, however the maximum lateral acceleration and sideslip angles are only a bit higher compared to the vehicle without TV.
The NMPC controller outperforms all of the controllers in terms of yaw rate performance, with the maximum way rate being 5% higher than the benchmark controllers and 11% higher than the vehicle without TV. The NMPC controller also has an increased lateral performance, which is 6 % higher than the benchmark controllers and 8% higher than the vehicle without TV. The NMPC controller uses a higher sideslip angle, utilising more grip from the tyre. The only downside of the NMPC controller is that the yaw rate tracking is 36% worse than the vehicle without torque vectoring comes and this difference becomes even bigger when compared to the benchmark controllers.

	$\dot{\psi}_{max}$ (deg/s)	RMS($e_{\dot{\psi}}$)(deg/s)	$a_{y,max}(m/s^2)$	$\beta_{max}(deg)$	$T_{max}(Nm)$
No TV	31.42	0.64	6.89	1,17	N/A
PD	32.89	0.12	6.94	1.22	246
LQR	33.26	0.24	7.00	1,14	252
NMPC	35.14	0.87	7.43	1.61	300

Table 7.2: Double lane change results for V_{in} = 50 km/h

In figure 7.4a, it is shown that the NMPC controlled vehicle is able to achieve a higher yaw rate in all turns. The yaw rate. for the PD, LQR and NO TV controller is similar. The yaw rate tracking of the PD controller is the best closely followed by the LQR Controller and they both outperform the vehicle without TV, as can be seen in figure 7.4b. The yaw rate tracking of the NMPC controller is worse than the benchmark controllers, as well as the vehicle without TV. Furthermore the yaw rate of the NMPC controller takes a while to get smooth at the last turn of the DLC manoeuvre.

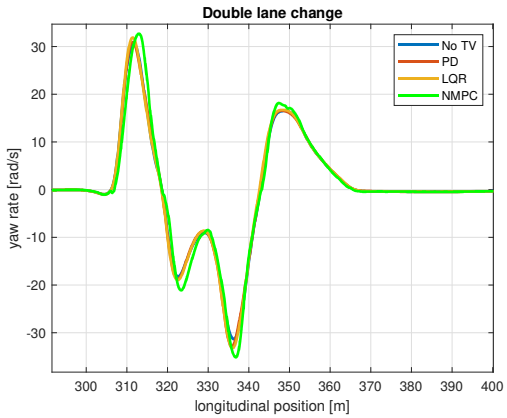

(a) Yaw rate of all controllers

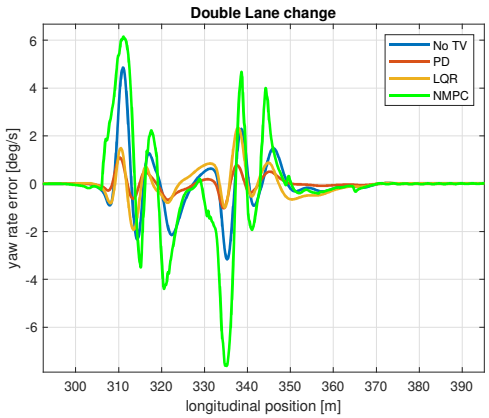

(b) Yaw rate error

Figure 7.4: Yaw rate plots of all the controllers

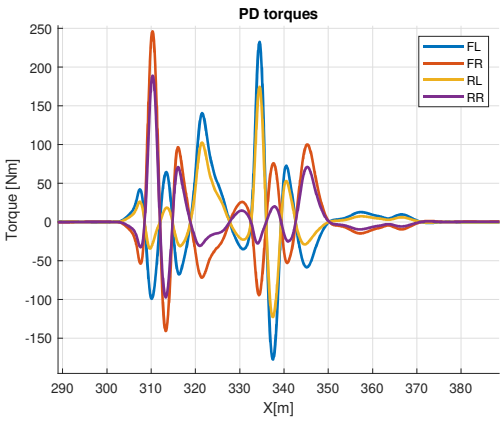

(a) Torques of the PD controller

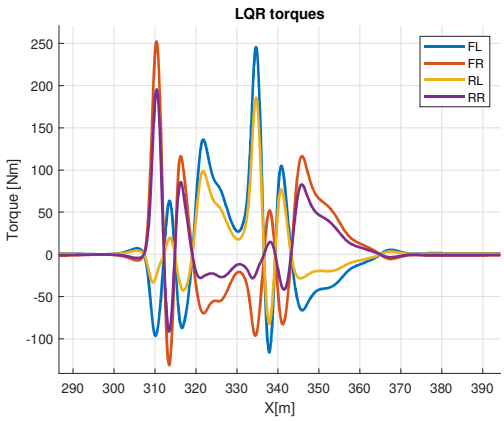

(b) Torques of the LQR controller

Figure 7.5: Plots of the torques for the various controllers

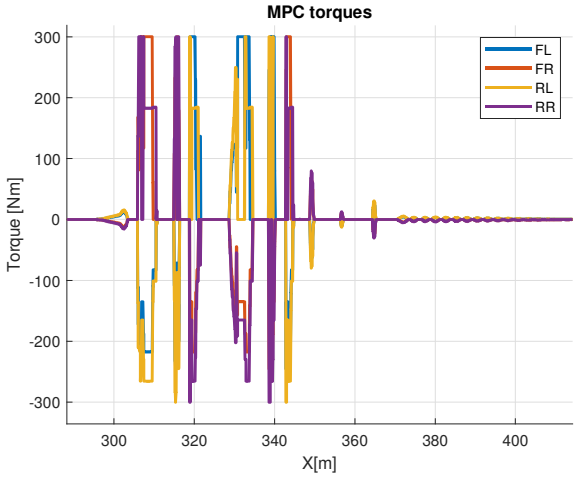

Figure 7.6: Torques from the MPC controller performing the DLC manoeuvre

The torque plots in figure 7.5 show that the both controllers are very similar in distributing the torques, with the peaks at 310, 320, 335 and 345 meters indicating the turns of the double lane change manoeuvre. In between these turns, the PD controller reduces its torques more quickly compared to the LQR controller, though both controllers are constantly using torques throughout the manoeuvre.

Looking at the torques in figures 7.5 and 7.6, one thing that is immediately noticeable is that the vehicle corrects itself from oversteer at around 315 meters after the first turn, which is also noticeable in the yaw rate error plot in figure 7.4b. The NMPC controller does this with a higher torques compared to the benchmark controllers, the same happens around 340 meters. The plots also show that the NMPC controller is more discrete with its torque application compared to the benchmark controllers and returns the torques quicker to zero compared to both benchmark controllers. This is due to the effect of the constraints from 4.11 and 4.12, where the direction of the torques are determined from the direction of the lateral acceleration.

7.2. Path Following Controllers

The double lane change manoeuvre is now used to compare the various types of path following controllers, where the vehicle starts with a velocity of 50 km/h.
The KPIs for the controller that only performs path following (denoted by PF only) and the controller that perform both path following and torque vectoring (denoted by PF + TV), are shown in table 7.3.

	$\dot{\psi}_{max}$ (deg/s)	RMS($e_{\dot{\psi}}$)(deg/s)	IA_{δ} (deg)	RMS(e_y)(m)
PF only	24.89	2.66	19.13	0.260
PF + TV	26.05	2.78	17.07	0.253

Table 7.3: Double lane change results for V_{in} = 50 km/h

From the KPI table it is noticeable that the PF + TV controller gets a higher maximum yaw rate, which is 5% higher than the PF controller. Reinforcing this is figure 7.7 where it can be seen that the PF+TV controller is able to get higher yaw rate peaks in all of the turns of the manoeuvre. However, this does come at the the expense of some yaw rate overshoot for the PF + TV controller after steering, though this overshoot does stay below 3 deg/s.
Another result from the KPI table is that PF only controller is slightly better at tracking the yaw rate reference, which is 1% lower. Figure 7.8 provides more context. In the corners, the PF + TV controller is better at yaw tracking, however after the corners, the PF controller is quicker in returning to zero yaw rate error, resulting in a better overall yaw rate tracking.

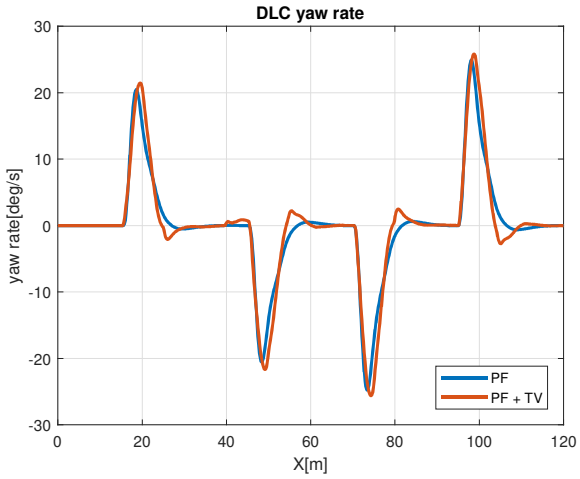

Figure 7.7: Yaw rate plots of both controllers

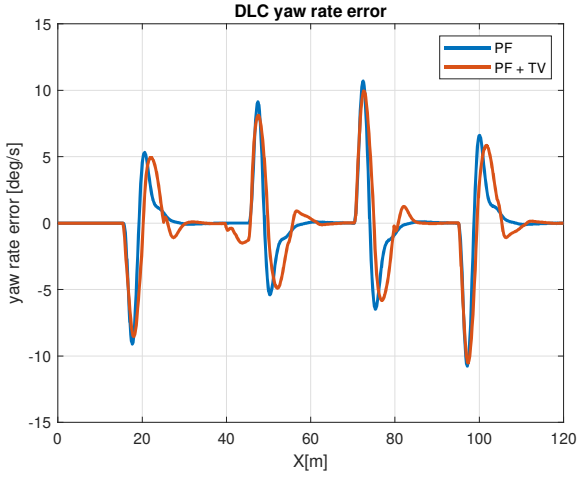

Figure 7.8: Yaw rate error plots of both controllers

The lateral tracking KPI shows that the PF+TV controller is better at path following than the PF controller by decreasing the lateral error with 4%. This is confirmed by the lateral error plot in figure 7.9, where the lateral error of the PF+TV controller is smaller than the PF controller throughout the manoeuvre.
Whilst the difference in the lateral error is noticeable, it is not big, as can be seen in figure 7.10a. The zoomed in path in figure 7.10b shows the difference, with the PF+TV controller having a higher overshoot after turn-in but has a lower settling time compared to the PF controller.

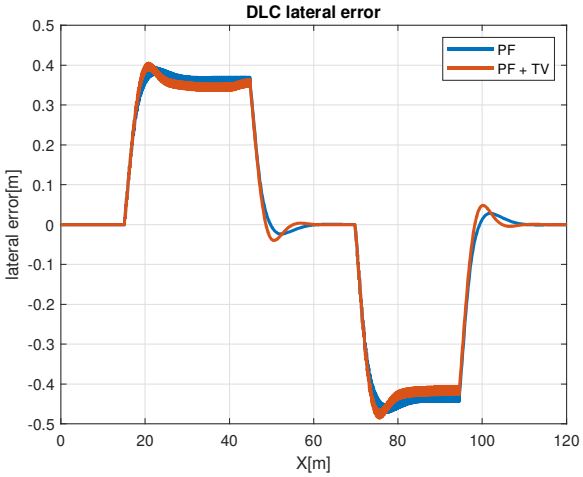

Figure 7.9: Lateral error plots of both controllers

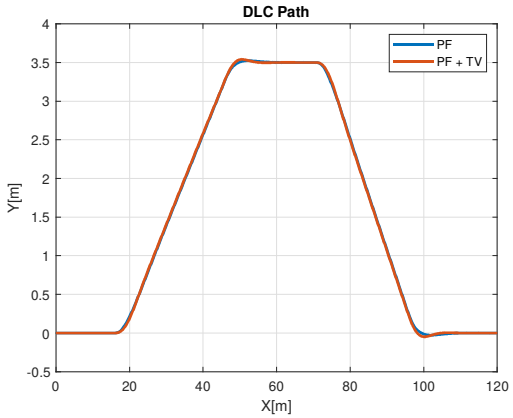

(a) Path

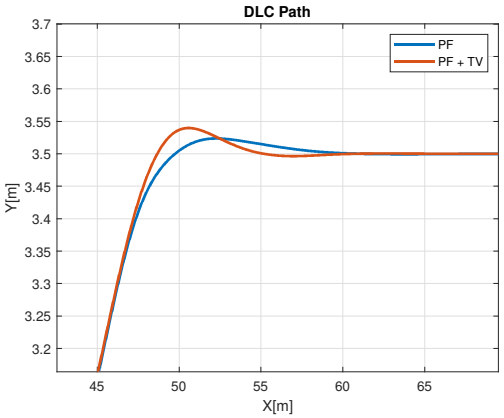

(b) Zoomed in path

Figure 7.10: Path plots of both controllers

Next, the results from the steering effort KPI show that the PF + TV controller decreases the overall steering angle by 11 % and the steering angle plot in figure 7.11 confirms that the PF+TV controller requires less steering angle. This is especially noticeable during cornering, where the PF+TV controller uses less steering angle everywhere. At corner exit, the PF+TV controller takes longer to returns to zero steering angle compared to the PF controlled vehicle.

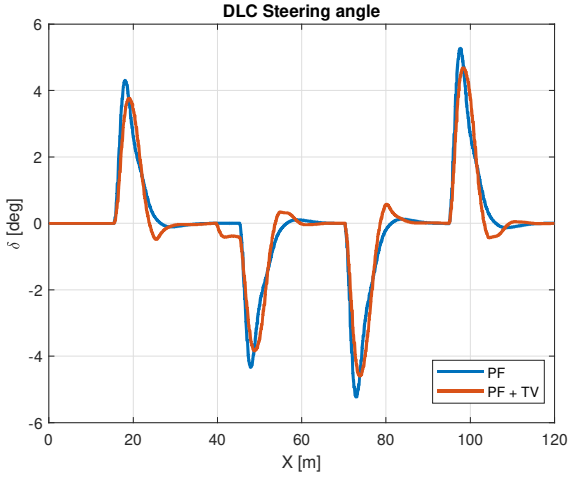

Figure 7.11: Steering angle plots of both controllers

In figure 7.12, it is noticeable that when the vehicle steers, that the controller applies the maximum amount of torque to turn the vehicle, which can be seen around 20,45,70 and 95 meters. Additional torque is applied around 20 and 80 meters in order to reduce the lateral error and a correcting torque is applied around 50 and 105 meters in order to correct the path overshoot and allows the vehicle to return to a orientation where the vehicle can move in a straight line. As a result, the PF+TV controlled vehicle has a lower settling time after cornering compared to the PF controlled vehicle.

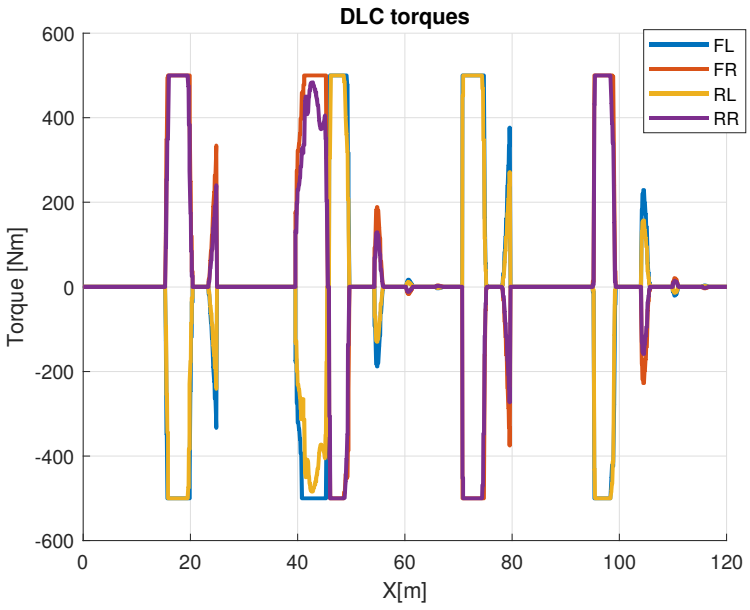

Figure 7.12: Torque of the PF + TV controller during the DLC manoeuvre

7.2.1. Yaw rate reference comparison

A comparison was also made between the existing yaw rate reference formulation from literature (3.35), which is denoted by PF+TV (old ref) and the new yaw rate reference formulation, established in (4.16), denoted by PF+TV (new ref). For both controllers, the double lane change manoeuvre was performed using the same parameters apart from the yaw rate reference and the yaw rate cost. In table 7.4, it can be seen from the KPIs that the controller with the new yaw rate reference increased the yaw rate by 1%, the steering effort is increased by 2% and the lateral error decreased by 1%. These are quite small differences. However, the yaw rate tracking improved with a bigger difference of 12%. This can also be seen in figure 7.13, where the yaw rate error of the new formulation is smaller throughout the manoeuvre and most noticeably in the corners.

	$\dot{\psi}_{max}$ (deg/s)	RMS($e_{\dot{\psi}}$)(deg/s)	IA_δ (deg)	RMS(e_y)(m)
PF +TV (new ref)	25.99	2.78	17.07	0.253
PF +TV (old ref)	25.70	3.17	16.70	0.254

Table 7.4: Double lane change results for V_{in} = 50 km/h

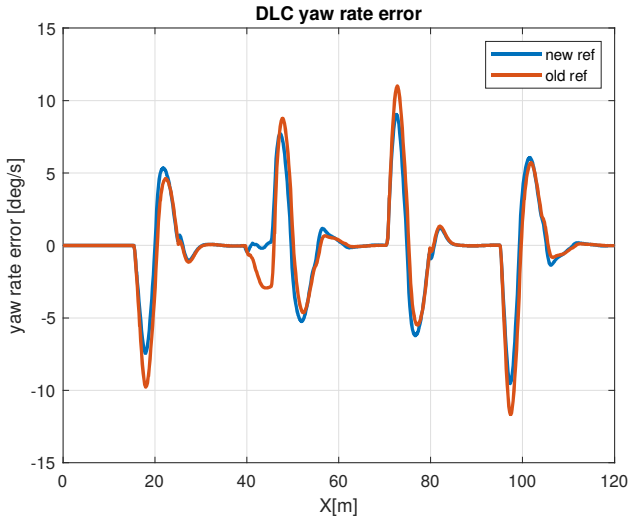

Figure 7.13: Yaw rate error plots of both formulations

7.2.2. Torque vectoring control without steering

Another comparison between the controllers was made by increasing the longitudinal distance of the double lane change manoeuvre. This was done as the controller that only uses torque vectoring to turn was not able to complete the manoeuvre in a stable manner for a shorter distance. The TV only controller is now able to complete the DLC manoeuvre in a stable manner now, though its path is oscillating as can be seen in figure 7.14. The reason for this can be seen in figures 7.16 and 7.17. As there is no steering available, the controller is using the maximum of its available torque, which is set to 700 Nm, to steer the vehicle. As it then somewhat over-corrects, it tries to send the torques the other way to keep the vehicle following the path, which is also why the yaw rate reference changes from side to side throughout the manoeuvre.

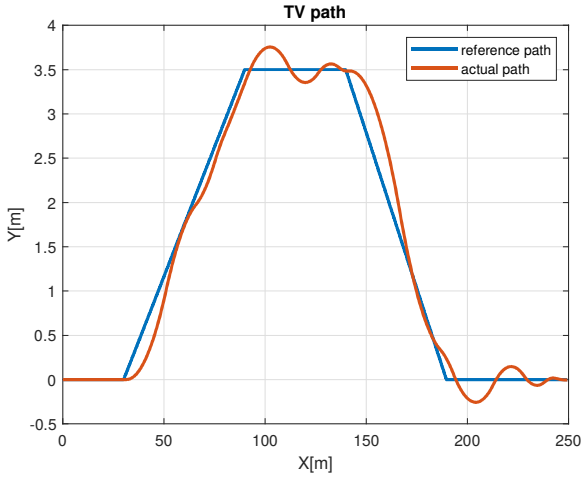

Figure 7.14: Path of TV only controller

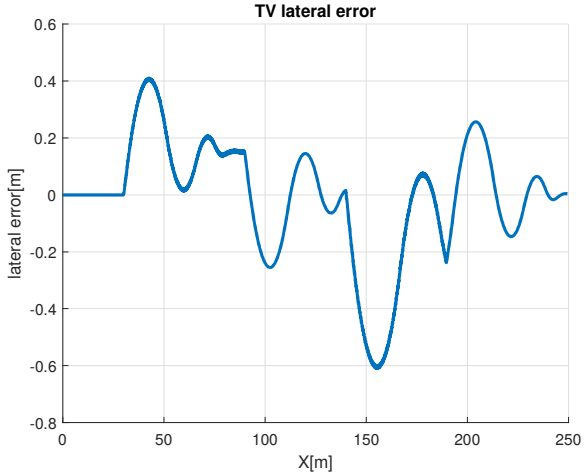

Figure 7.15: Lateral error of TV only controller

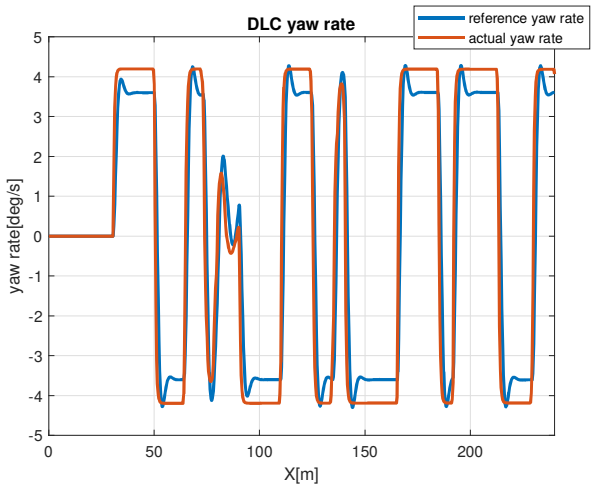

Figure 7.16: Yaw rate of TV only controller

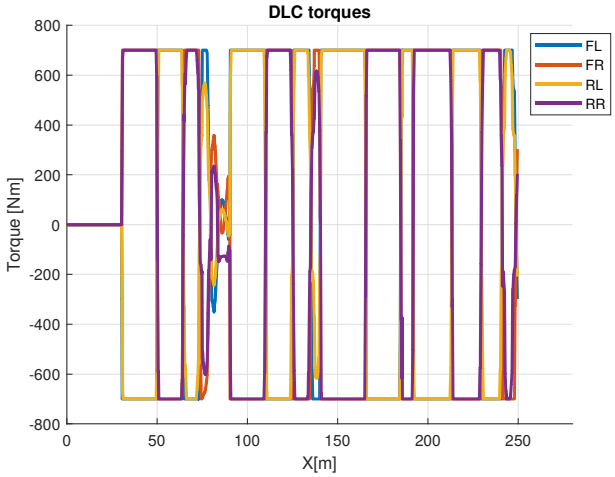

Figure 7.17: Torques of TV only controller

The result of having a vehicle that is steered by torques only is that compared to the other controllers, that this controller is outperformed in every metric by the path following controllers that do include a steering angle, as seen in table B.3. The maximum yaw rate is three times lower than the PF controller, as well as roughly doubling the tracking error for both the yaw rate tracking, as well as the lateral tracking performance.

	$\dot{\psi}_{max}$ (deg/s)	RMS($e_{\dot{\psi}}$)(deg/s)	RMS(e_y)(m)
PF only	12.22	0.95	0.131
TV only	4.19	2.12	0.215
PF +TV	14.13	1.48	0.122

Table 7.5: Double lane change results for V_{in} = 50 km/h with increased longitudinal distance

7.3. Discussion

7.3.1. Benchmark controllers vs NMPC controller

Starting with the SwD manoeuvre, all torque vectoring controllers manage to outperform the vehicle without TV in all metrics, so the benefit of torque vectoring is confirmed here. When comparing the NMPC controller with the benchmark controllers, the results show that the NMPC controller has similar peak yaw rates and lateral acceleration, whilst having worse yaw rate tracking and a similar sideslip angle. With the benchmark controllers being near the maximum yaw rate and having a fixed input for the steering angle, it is always a challenge to outperform these controllers. Tuning the weights for the NMPC controller did not lead to improvements, as setting the weight for the yaw rate too high created a yaw rate that would become noisier. Setting the yaw rate weight lower decreased the lateral performance and the yaw rate tracking.

When looking at the double lane change manoeuvre the results changed. All of the TV controllers managed to outperform the vehicle without TV again in all metrics, with the exception being the NMPC controller having a worse yaw rate tracking. The PD and LQR controller have a somewhat better yaw rate and lateral performance compared to the vehicle without TV and a near perfect yaw rate tracking, whilst maintaining a similar maximum sideslip angle. However, the NMPC controller has a higher lateral performance and yaw rate performance compared to the benchmark controllers. This comes at a cost of a lower yaw rate tracking performance. The reason for this is that the NMPC controller had a small delay in following the yaw rate reference, whilst still achieving similar peak yaw rates. Nevertheless, the NMPC controller was able to utilise more of the tyres than both of the benchmark controllers for the double lane change manoeuvre and get more lateral performance as a result.

7.3.2. Path following controllers

Comparing the PF only controller, with the PF + TV controller, it can be observed that the PF + TV controller is beneficial when performing the DLC manoeuvre. This is seen in both the yaw rate performance, as well as the lateral tracking. The yaw rate tracking of both controllers is similar. Another benefit of TV is also that less steering angle is required, which is in line with the literature that torque vectoring improves the responsiveness of the vehicle. This shows that path following and torque vectoring can be performed using the NMPC controller and that torque vectoring can help with performing path following.

When the TV controllers with the different yaw rate reference formulations are compared, the results show that both formulation perform similarly in most metrics. However, when the yaw rate tracking of both formulations is compared, it becomes clear that the controller with the yaw rate reference formulation that includes the yaw moment from torque vectoring outperforms the yaw rate reference formulation that only uses the steering angle as an input.

Finally, whilst the controller that steers by torque vectoring only is outperformed by the other controllers in every metric, the TV only controller is still able to complete the double lane change manoeuvre. though it does this by continuously changing the direction of the torques.

8

Conclusion

8.1. Conclusions

8.1.1. Torque vectoring controllers

During this thesis, different torque vectoring controllers were designed and assessed. The NMPC TV controller was compared to the benchmark controllers and a vehicle without TV, which were established in the literature. To evaluate the controllers, scenarios such as the the sine with dwell test and double lane change manoeuvre were used. When the simulations were completed, a comparison of the controllers was made by using KPIs, which consisted of yaw rate tracking, stability, lateral performance and manoeuvrability. In both scenarios it becomes clear that adding torque vectoring improves the vehicle performance across all metrics.

When the NMPC controlled vehicle was compared to the benchmark controllers, the results show that during the sine with dwell manoeuvre that the NMPC controller is not able to improve the performance of the vehicle. In this scenario the KPIs were similar apart from the reference yaw rate tracking performance, which was worse for the NMPC controller. This is because the benchmark controllers are able to get the yaw rate of the vehicle near the limit of the yaw rate constraint which makes it difficult for the NMPC controller to improve upon. However, the double lane change manoeuvre is a manoeuvre where the vehicle is not near limit of the yaw rate constraint. Therefore, the NMPC controller is able to increase the lateral performance and achieve higher manoeuvrability, when compared to the benchmark controllers at the expense of worse yaw rate tracking. When tuning the NMPC controller for these manoeuvres, it was always a compromise between improving the yaw rate tracking or improving the lateral performance and vehicle handling.

8.1.2. Path following controllers

Furthermore, different formulations of the NMPC controller were tested and evaluated to perform path following. The formulations that were compared included one where the vehicle input is only its steering angle and second one where the vehicle can only steered by wheel torques and finally a formulation where the vehicle is steered by both the steering wheel and torque vectoring. The scenario that was chosen for this comparison is the double lane change manoeuvre.

When torque vectoring was added to the control strategy, it improved the vehicle performance in terms of agility, lateral performance, responsiveness and slightly better path following when compared to a vehicle with TV. The yaw rate tracking for both controllers was similar. By adding the yaw moment that is generated by torque vectoring in the reference yaw rate formulation, the yaw rate tracking of the vehicle improved whilst performing similarly on the other metrics.

Finally, steering the vehicle by torque vectoring only is not an easy task. The torques needed to be increased, compared to the vehicle that uses both a steering angle and torque vectoring, for the vehicle to somewhat follow the path. Whilst the performance of the controller that only steers by torques is

worse than the other controllers, it is still important to note that the vehicle is still able to follow the path by steering with torques only.

8.2. Recommendations

During this thesis the cost function weights for the MPC controller were manually tuned. The plots and KPIs were used in order to improve the cost function weights. However, first of all it can not be determined whether this leads to a local or global optimum. Furthermore, the weight tuning needs to be done for different manoeuvres and velocities. One way this can be solved is by including variable tuning for the cost function weights. Weights can be set that prioritise yaw rate tracking, path following or a compromise that balances between both. The variable tuning can be done by the use of a fuzzy controller, of which an example can be found in [16].

Another aspect that can be tested is by getting the NMPC PF controller to work with various vehicles and tyre models, either in CarMaker or other simulation software. First of all, because the vehicle behaviour will be simulated more accurately in a vehicle simulation software than in Simulink and in order to confirm the benefits of torque vectoring and nonlinear model predictive control across multiple use cases. This can then be extended to be implemented in a real vehicle in order to see whether there is a good correlation between the simulation results and real world data.

Additionally, another test that can be made is to adjust the road-tyre friction coefficient to compare the NMPC controller with the other controllers in lower grip conditions. Whilst this has been done in the literature for torque vectoring only, this has not been done for a NMPC controller that integrates both torque vectoring and path following.

Finally, adding the torque times lateral acceleration constraints (equations (4.11) and (4.12)) improved the torque distribution, as the controller now always allocates the wheel torques to the correct side of the vehicle, whereas before the controller would switch the sides of the torques constantly, even during steady-state cornering. The only caveat is that whilst this worked great for the double lane change manoeuvre, it did not adhere to this constraint during the sine with dwell manoeuvre. Therefore, it is recommended to introduce slack variables to these constraints or alternatively, try and write these constraints in a similar form as part as a cost function instead of hard constraints.

Bibliography

[1] Ministerie van Infrastructuur en Waterstaat. *Self-driving vehicles*. 2020. URL: https://www.government.nl/topics/mobility-public-transport-and-road-safety/self-driving-vehicles.

[2] *e Torque Vectoring*. 2023. URL: https://www.hoferpowertrain.com/technology-page/e-torque-vectoring.

[3] Bing Zhang et al. "Electrical Vehicle Path Tracking Based Model Predictive Control With a Laguerre Function and Exponential Weight". In: *IEEE Access* 7 (2019), pp. 17082–17097. DOI: 10.1109/access.2019.2892746. URL: https://doi.org/10.1109%2Faccess.2019.2892746.

[4] Jonathan C. Wheals et al. "Torque Vectoring AWD Driveline: Design, Simulation, Capabilities and Control". In: *SAE Technical Paper Series*. SAE International, Mar. 2004. DOI: 10.4271/2004-01-0863. URL: https://doi.org/10.4271%2F2004-01-0863.

[5] Valentin Ivanov, Klaus Augsburg, and Dzmitry Savitski. "Torque vectoring for improving the mobility of all-terrain electric vehicles". In: *Proceedings of the European Regional Conference of the International Society for Terrain-Vehicle-Systems*. 2012, pp. 1–8. URL: https://www.researchgate.net/publication/236216875_Torque_vectoring_for_improving_the_mobility_of_all-terrain_electric_vehicles.

[6] R Freimann, TM Wolter, and E Schneider. "Driving Dynamics and hybrid combined in the torque vectoring–Concepts of axle differentials with hybrid functionality and active torque distribution". In: *Vehicle Dynamics Expo* (2009).

[7] Aldo Sorniotti, Phil Barber, and Stefano De Pinto. "Path Tracking for Automated Driving: A Tutorial on Control System Formulations and Ongoing Research". In: *Automated Driving*. Springer International Publishing, Sept. 2016, pp. 71–140. DOI: 10.1007/978-3-319-31895-0_5. URL: https://doi.org/10.1007%2F978-3-319-31895-0_5.

[8] Paolo Falcone et al. "Predictive Active Steering Control for Autonomous Vehicle Systems". In: *IEEE Transactions on Control Systems Technology* 15.3 (May 2007), pp. 566–580. DOI: 10.1109/tcst.2007.894653. URL: https://doi.org/10.1109%2Ftcst.2007.894653.

[9] Christoforos Chatzikomis et al. "Comparison of Path Tracking and Torque-Vectoring Controllers for Autonomous Electric Vehicles". In: *IEEE Transactions on Intelligent Vehicles* 3.4 (Dec. 2018), pp. 559–570. DOI: 10.1109/tiv.2018.2874529. URL: https://doi.org/10.1109%2Ftiv.2018.2874529.

[10] Wenliang Zhang et al. "Evaluating Model Predictive Path Following and Yaw Stability Controllers for Over-Actuated Autonomous Electric Vehicles". In: *IEEE Transactions on Vehicular Technology* 69.11 (Nov. 2020), pp. 12807–12821. DOI: 10.1109/tvt.2020.3030863. URL: https://doi.org/10.1109%2Ftvt.2020.3030863.

[11] M Heemels. *MPC and Constrained Systems*. 2013. URL: https://heemels.tue.nl/research/mpc-and-constrained-systems.

[12] Efstathios Siampis, Efstathios Velenis, and Stefano Longo. "Rear wheel torque vectoring model predictive control with velocity regulation for electric vehicles". In: *Vehicle System Dynamics* 53.11 (July 2015), pp. 1555–1579. DOI: 10.1080/00423114.2015.1064972. URL: https://doi.org/10.1080%2F00423114.2015.1064972.

[13] J.M. Maciejowski. *Predictive Control with Constraints.* England.: Prentice Hall, 2002.

[14] Efstathios Siampis, Efstathios Velenis, and Stefano Longo. "Model Predictive torque vectoring control for electric vehicles near the limits of handling". In: *2015 European Control Conference (ECC)*. IEEE, July 2015. DOI: 10.1109/ecc.2015.7330922. URL: https://doi.org/10.1109%2Fecc.2015.7330922.

[15] Alberto Parra et al. “On Nonlinear Model Predictive Control for Energy-Efficient Torque-Vectoring”. In: *IEEE Transactions on Vehicular Technology* 70.1 (Jan. 2021), pp. 173–188. DOI: 10.1109/tvt.2020.3022022. URL: https://doi.org/10.1109%2Ftvt.2020.3022022.

[16] Matteo Dalboni et al. “Nonlinear Model Predictive Control for Integrated Energy-Efficient Torque-Vectoring and Anti-Roll Moment Distribution”. In: *IEEE/ASME Transactions on Mechatronics* 26.3 (June 2021), pp. 1212–1224. DOI: 10.1109/tmech.2021.3073476. URL: https://doi.org/10.1109%2Ftmech.2021.3073476.

[17] Leonardo De Novellis et al. “Torque Vectoring for Electric Vehicles with Individually Controlled Motors: State-of-the-Art and Future Developments”. In: *World Electric Vehicle Journal* 5.2 (June 2012), pp. 617–628. DOI: 10.3390/wevj5020617. URL: https://doi.org/10.3390%2Fwevj5020617.

[18] *Passenger cars — Validation of vehicle dynamic simulation — Sine with dwell stability control testing*. Standard. London, U.K.: British Standards Institution, 2016. DOI: 10.3403/30293119u. URL: https://doi.org/10.3403%2F30293119u.

[19] Karan Chatrath. “Vehicle Dynamics Control Using Control Allocation”. PhD thesis. July 2019. DOI: 10.13140/RG.2.2.35878.65608.

[20] *Passenger Cars—Test Track for a Severe Lane-Change Manoeuvre Part 2: Obstacle Avoidance*. Standard. London, U.K.: British Standards Institution, 2011. DOI: 10.3403/02743307u. URL: https://doi.org/10.3403%2F02743307u.

A

Vehicle parameters

Parameter	Description	Value	Unit
m	Mass	1620	kg
I_{zz}	Moment of inertia around z-axis	2840	Nm
L	Wheelbase	2.8	m
l_f	Distance from front axle to CoG	1.055	m
h_{CG}	CoG height	0.549	m
t_w	Trackwidth	1.58	m
$h_{roll,f}$	Front roll centre height	0.098	m
$h_{roll,r}$	Rear roll centre height	0.061	m
R	Wheel effective radius	0.3285	m
I_ω	Wheel moment of inertia	0.847	Nm
i_{steer}	Steering radio	18.44	-
$C_{\alpha f}$	Front axle cornering stiffness	125000	Nm/rad
$C_{\alpha r}$	Rear axle cornering stiffness	180000	Nm/rad
$f_{T,L,opt}$	Front-to-total torque distribution left side	0.6	-
$f_{T,R,opt}$	Front-to-total torque distribution right side	0.6	-

Table A.1: Vehicle parameter table

Parameter	Description	Value
ω_n	yaw frequency	14.5
$\omega_{n,0}$	yaw delay	0.002
ζ	yaw damping	0.6

Table A.2: Second-order transfer function parameters of the dynamic yaw rate reference response

B

Cost function weights

B.1. TV weights

The PD weights for both the sine with dwell manoeuvre (denoted by SwD) and the double lane change manoeuvre (denoted by DLC) are given below:

	K_p	K_d
SWD	6	0.4
DLC	100	0.25

Table B.1: Values of the PD gains

The LQR controller weights are described below, where Q is the state weighting matrix, with the two states being the lateral velocity and the yaw rate and R is the input vector, which is the yaw moment. Equation B.1 refers to to weights for the sine with dwell manoeuvre and equation B.2 refers to to weights for the double lane change manoeuvre.

$$Q = \begin{bmatrix} 1 * 10^9 & 0 \\ 0 & 1 * 10^9 \end{bmatrix} \qquad R = 8 \tag{B.1}$$

$$Q = \begin{bmatrix} 1 * 10^9 & 0 \\ 0 & 1 * 10^8 \end{bmatrix} \qquad R = 0.01 \tag{B.2}$$

	$\dot{\psi}$	T_{diff}	T_{total}
SWD Stage cost	$3 * 10^4$	$1 * 10^{-3}$	$1 * 10^{-6}$
SWD Terminal cost	$6 * 10^3$	N/A	N/A
DLC Stage cost	$1 * 10^5$	$8 * 10^3$	$5 * 10^{-1}$

Table B.2: Cost function weights for the MPC controller

B.2. PF weights

	$\dot{\psi}$	Y_p	T_{diff}	T_{total}	$\dot{\delta}$
PF only	0	300	0	0	5
PF +TV	$1 * 10^3$	$5 * 10^4$	$2 * 10^{-3}$	1	$1 * 10^3$

Table B.3: Stage cost function weights for PF controllers at the double lane change

	$\dot{\psi}$	Y_p	T_{diff}	T_{total}	$\dot{\delta}$
TV only	$2 * 10^4$	$5 * 10^5$	$1 * 10^{-2}$	1	0

Table B.4: Stage cost function weights for PF controllers that steers by TV alone at double lane change

C

Derivation of yaw rate reference based on yaw moment from TV

C.1. Yaw rate reference derivation

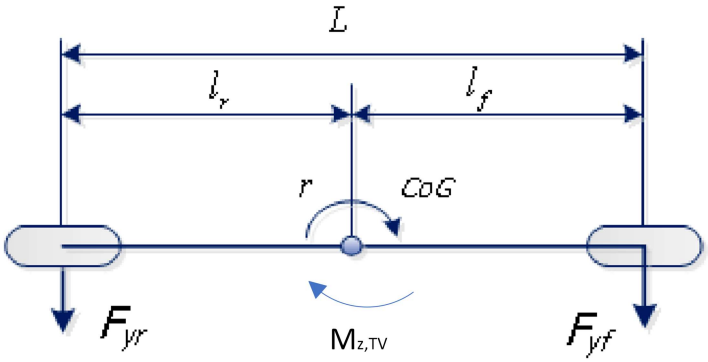

Figure C.1: Bicycle model with added yaw moment from torque vectoring

Now, the TV yaw moment is added to the moment balance around the z-axis as follows:

$$\sum M_z = l_f F_{yf} + M_{z,TV} - l_r F_{yr} = 0 \tag{C.1}$$

With the lateral force balance being given by:

$$\sum F_y = F_{yf} + F_{yr} \tag{C.2}$$

The moment balance equation is rewritten in (C.3) as a function of F_{yf}. Then, the substitution of (C.3) in (C.2) result in (C.4) and (C.5).

$$F_{yf} = \frac{l_r}{l_f} F_{yr} - \frac{M_{z,TV}}{l_f} \tag{C.3}$$

$$F_{yr} = \frac{l_f}{L}\left(\frac{mu^2}{R} + \frac{M_{z,TV}}{l_f}\right) \tag{C.4}$$

$$F_{yf} = \frac{l_r}{L}\left(\frac{mu^2}{R} + \frac{M_{z,TV}}{l_f}\right) - \frac{M_{z,TV}}{l_f} \tag{C.5}$$

Now that the lateral forces are written in terms of the added yaw moment by TV, the steering law for steady-state cornering can be rewritten into:

$$\delta = \frac{L}{R} + \frac{ml_r u^2}{LRC_{\alpha f}} - \frac{ml_f u^2}{LRC_{\alpha r}} + \frac{M_{z,TV} l_r}{Ll_f C_{\alpha f}} - \frac{M_{z,TV}}{l_f C_{\alpha f}} - \frac{M_{z,TV}}{LC_{\alpha r}} \tag{C.6}$$

The second part of the equation that contains the added yaw moment is rewritten into one term through equations (C.7) and (C.8).

$$\frac{M_{z,TV} l_r}{Ll_f C_{\alpha f}} - \frac{M_{z,TV}}{l_f C_{\alpha f}} = -\frac{M_{z,TV}}{LC_{\alpha f}} \tag{C.7}$$

$$\frac{M_{z,TV}}{LC_{\alpha f}} + \frac{M_{z,TV}}{LC_{\alpha r}} = \frac{M_{z,TV}(C_{\alpha f} + C_{\alpha r)}}{LC_{\alpha f} C_{\alpha r}} \tag{C.8}$$

This results into a more simplified expression for the steering law:

$$\delta = \frac{L}{R} + \frac{mu^2}{LR}\left(\frac{l_r}{C_{\alpha f}} - \frac{l_f}{C_{\alpha r}}\right) - \frac{M_{z,TV}(C_{\alpha f} + C_{\alpha r)}}{LC_{\alpha f} C_{\alpha r}} \tag{C.9}$$

As $R = \frac{u}{r}$, with *R* being the corner radius, *u* being the longitudinal velocity and *r* being the yaw rate, the steering law is then rewritten as:

$$\delta = \frac{Lr}{u} + \frac{mru}{L}\left(\frac{l_r}{C_{\alpha f}} - \frac{l_f}{C_{\alpha r}}\right) - \frac{M_{z,TV}(C_{\alpha f} + C_{\alpha r)}}{LC_{\alpha f} C_{\alpha r}} \tag{C.10}$$

Theoretically it should be possible for the vehicle to steer by just using TV as this creates a yaw moment allowing the vehicle to rotate, which can help in for path following. For this case, the assumption is made that the steer wheel angle is 0, which results in the equation becoming:

$$r\left(\frac{L}{u} + \frac{mu}{L}\left(\frac{l_r}{C_{\alpha f}} - \frac{l_f}{C_{\alpha r}}\right)\right) = \frac{M_{z,TV}(C_{\alpha f} + C_{\alpha r})}{LC_{\alpha f} C_{\alpha r}} \tag{C.11}$$

This can then be rewritten into a function of: $\frac{r}{M_{z,TV}}$:

$$\frac{r}{M_{z,TV}} = \frac{C_{\alpha f} + C_{\alpha r}}{LC_{\alpha f} C_{\alpha r}} \frac{u}{L + \frac{mu^2}{L}\left(\frac{l_r}{C_{\alpha f}} - \frac{l_f}{C_{\alpha r}}\right)} \tag{C.12}$$

The equation is then rewritten in terms of the understeer gradient:

$$\frac{r}{M_{z,TV}} = \frac{(C_{\alpha f} + C_{\alpha r})u}{LC_{\alpha f} C_{\alpha r}\left(L + \frac{K_{us} u^2}{g}\right)} \tag{C.13}$$

Therefore as a result the yaw rate reference is written is terms of the added yaw moment by TV:

$$\dot{\psi}_{ss} = \frac{(C_{\alpha f} + C_{\alpha r})u}{LC_{\alpha f} C_{\alpha r}\left(L + \frac{K_{us} u^2}{g}\right)} M_{z,TV} \tag{C.14}$$

C.2. Yaw moment from TV equations

In order to determine the yaw rate reference, the yaw moment that is added by torque vectoring needs to be calculated. This is at first done by calculating the yaw moment at the front in (C.15). Then, for simplification the assumption is made that the torques are applied proportionally to the vertical loads of the wheels from which the yaw moment from TV is calculated in (C.16).

$$M_{z,f} = \frac{T_{f,i} t_w}{R_{eff}} \tag{C.15}$$

$$M_{z,TV} = \frac{M_{z,f} \sum F_z}{\sum F_{z,f}} \tag{C.16}$$

D

PF Vehicle model

The vehicle model that is created in Simulink is based on Dalboni's paper [16]. The main difference is that only front wheel steering has been used in this research compared to the all wheel steering in Dalboni's paper. To get the results the vehicle model and tyre model from chapter 3 is used.

The yaw moment balance is given by:

$$\begin{aligned}\ddot{\psi} =& \frac{1}{I_{zz}} l_f[(F_{x,FL} + F_{x,FR}sin(\delta)) + (F_{y,FL} + F_{y,FR}cos(\delta))] - l_r[F_{y,FL} + F_{y,FR}] \\ &+ \frac{t_w}{2}[(F_{x,FR} - F_{x,FL}cos(\delta) + (F_{y,FL} - F_{y,FR}sin(\delta) - F_{x,RL} + F_{x,RR}]\end{aligned} \tag{D.1}$$

where I_{zz} is the moment of inertia around the z-axis, l_f and l_r are the distance from the front and rear axis to the vehicle CoG respectively and t_w is the vehicle track width.

Next, the wheel moment balance is given as:

$$\dot{\omega}_j = \frac{1}{I_\omega} T_j - F_{x,j} R \tag{D.2}$$

where I_ω is the wheel moment of inertia, T_{ij} is the wheel torque and *R* is the effective wheel radius. The subscript *j* denotes the tyre where 1 is the front left, 2 the front right, 3 the rear left and 4 the rear right.

Formulations for both the change in longitudinal and lateral positions and the yaw rate given below:

$$\dot{X}_p = v_x \cos\psi - v_y \sin\psi \tag{D.3}$$

$$\dot{Y}_p = v_x \sin\psi + v_y \cos\psi \tag{D.4}$$

$$\dot{\psi} = \dot{\psi} \tag{D.5}$$

The longitudinal and lateral force balances are given below:

The longitudinal force balance:

$$\dot{V} = \frac{1}{m}[cos(\beta)(\sum_{j=1}^{4} F_{x,j}cos(\delta) - F_{y,j}sin(\delta)) + sin(\beta)(\sum_{j=1}^{4} F_{x,j}sin(\delta) + F_{y,j}cos(\delta))] \quad \text{(D.6)}$$

The lateral force balance:

$$\dot{\beta} = \frac{1}{mV}[cos(\beta)(\sum_{j=1}^{4} F_{x,j}sin(\delta) + F_{y,j}cos(\delta)) - sin(\beta)(\sum_{j=1}^{4} F_{x,j}sin(\delta) - F_{y,j}cos(\delta))] - \dot{\psi} \quad \text{(D.7)}$$

The longitudinal acceleration a_x and lateral acceleration a_y are approximations from the bicycle given below:

$$a_x = -v_y * \dot{\psi} \quad \text{(D.8)}$$

$$a_y = v_x * \dot{\psi} \quad \text{(D.9)}$$

E

Yaw rate reference comparison plots

The plots that are given below compare the yaw rate reference formulations where *old ref* is the yaw rate reference with the steering angle as an input and *new ref* is the reference that uses the steering angle and yaw moment generated by torque vectoring as inputs. These plots are in the appendix because the differences between both formulations are small as seen in KPI table 7.4.

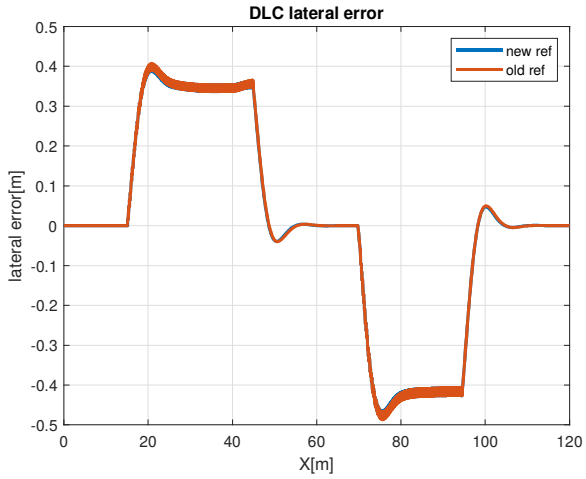

Figure E.1: Lateral error plots of both formulations

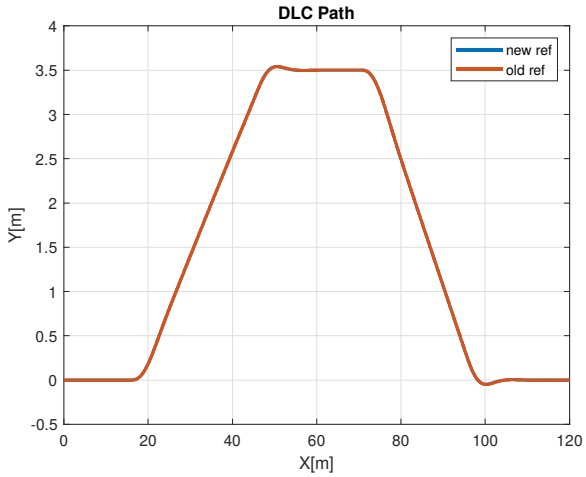

Figure E.2: Path plots of both formulations

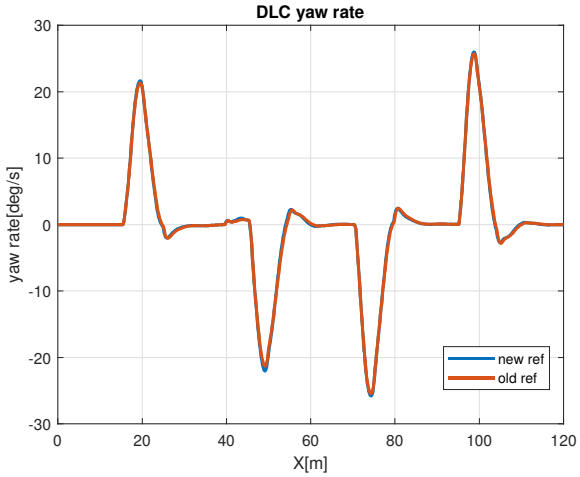

Figure E.3: Yaw rate plots of both formulations

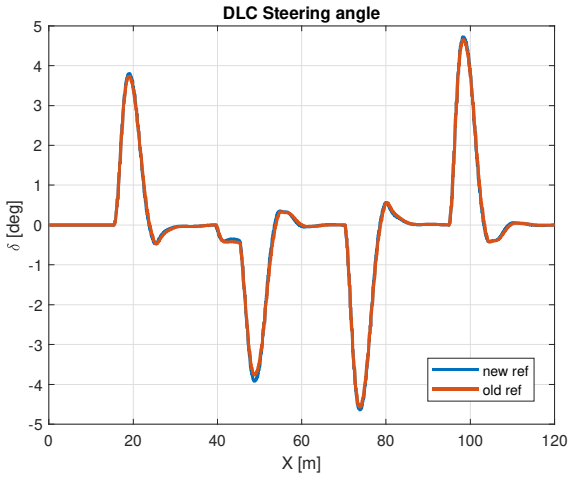

Figure E.4: Steering angle plots of both formulations